



1 **Measurement report: Enhanced photochemical formation of**
2 **formic and isocyanic acids in urban region aloft: insights**
3 **from tower-based online gradient measurements**

4 Qing Yang^{1,2}, Xiao-Bing Li^{1,2,*}, Bin Yuan^{1,2,*}, Xiaoxiao Zhang^{1,2}, Yibo Huangfu^{1,2}, Lei
5 Yang^{1,2}, Xianjun He^{1,2}, Jipeng Qi^{1,2}, Min Shao^{1,2}

6 ¹ Institute for Environmental and Climate Research, Jinan University, Guangzhou
7 511443, China

8 ² Guangdong-Hongkong-Macau Joint Laboratory of Collaborative Innovation for
9 Environmental Quality, Guangzhou 511443, China

10 * Corresponding authors: Xiao-Bing Li (lixiaobing@jnu.edu.cn), Bin Yuan
11 (byuan@jnu.edu.cn)



12 **Abstract**

13 Formic acid is the most abundant organic acid in the troposphere and has
14 significant environmental and climatic impacts. Isocyanic acid poses severe threats to
15 human health and could be formed through the degradation of formic acid. However,
16 the lack of vertical observation information has strongly limited the understanding of
17 their sources, particularly in urban regions with complex pollutant emissions. To
18 address this issue, continuous (27 days) vertical gradient measurements (five heights
19 between 5-320 m) of formic and isocyanic acids were made based on a tall tower in
20 Beijing, China in summer of 2021. Results show that the respective mean mixing ratios
21 of formic and isocyanic acids were 1.3 ± 1.3 ppbv and 0.28 ± 0.16 ppbv at 5 m and were
22 2.1 ± 1.9 ppbv and 0.43 ± 0.21 ppbv at 320 m during the campaign. The mixing ratios of
23 formic and isocyanic acids were substantially enhanced in daytime and correlated with
24 the diurnal change of ozone. Upon sunrise, the mixing ratios of formic and isocyanic
25 acids at different heights simultaneously increased even in the residual layer. In addition,
26 positive vertical gradients were observed for formic and isocyanic acids throughout the
27 day. The afternoon peaks and positive vertical gradients of formic and isocyanic acids
28 in nighttime indicate their dominant contributions from photochemical formations.
29 Furthermore, the positive vertical gradients of formic and isocyanic acids in daytime
30 imply the enhancement of their secondary formation in urban regions aloft,
31 predominantly due to the enhancements of oxygenated volatile organic compounds.
32 The formation pathway of isocyanic acid through $\text{HCOOH-CH}_3\text{NO-HNCO}$ was
33 enhanced with height but only accounted for a tiny fraction of its ambient abundance.
34 The abundance and source contributions of formic and isocyanic acids in the
35 atmospheric boundary layer may be highly underestimated when being derived from
36 their ground-level measurements. With the aid of numerical modeling techniques,
37 future studies could further identify key precursors that drive the rapid formation of
38 formic and isocyanic acids, and quantitatively assess the impacts of the enhanced
39 formation of the two acids aloft on their budgets at ground level.



40 **1. Introduction**

41 Formic acid (HCOOH) is the simplest but the most abundant organic acid in the
42 troposphere. It has been widely measured in aqueous (clouds and aerosols) and gaseous
43 phases over urban, rural, and remote regions (*Kawamura and Kaplan, 1983; Chebbi*
44 *and Carlier, 1996; Kesselmeier et al., 1998; Yu, 2000*). As important contributors to the
45 acidity of precipitation, formic and acetic acids can account for 60% of the free acidity
46 in remote regions (*Galloway et al., 1982; Andreae et al., 1988*), and over 30% of the
47 free acidity in heavily polluted regions (*Keene and Galloway, 1984*). Formic acid is
48 also an important sink of hydroxyl radicals (OH) in clouds (*Jacob, 1986*), playing vital
49 roles in modulating the atmospheric aqueous-phase chemistry through changing pH-
50 dependent reaction rates of related constituents. An in-depth understanding of the
51 concentration levels, spatiotemporal variations, and sources of formic acid is key to
52 elucidating the formation mechanisms of atmospheric secondary pollution. However,
53 the sources and sinks of atmospheric formic acid are still poorly understood so far.

54 There have been many reported sources of atmospheric formic acid. Primary
55 emissions from vegetation activity (*Andreae et al., 1988; Kesselmeier et al., 1998*),
56 microbial metabolism (*Enders et al., 1992*), biomass burning (*Goode et al., 2000*), and
57 vehicle exhaust (*Kawamura et al., 2000*) were identified as important sources of formic
58 acid. Secondary formation from photochemical degradation of volatile organic
59 compounds (VOCs) is another significant source of formic acid (*Khare et al., 1999;*
60 *Veres et al., 2011; Le Breton et al., 2014; Liggio et al., 2017*). However, current
61 chemical transport models still highly underestimate ambient concentrations of formic
62 acid (*Stavrakou et al., 2011; Paulot et al., 2011; Millet et al., 2015*) and cannot well
63 reproduce its vertical variations. For example, *Mattila et al. (2018)* measured vertical
64 profiles of formic acid using an elevator on the Colorado Front Range BOA tower. They
65 found that formic acid mixing ratios generally decreased with height throughout the day,
66 but there were no known sources to explicitly explain the net surface emissions. The
67 vertical distribution and variation patterns of formic acid in the atmospheric boundary



68 layer can provide valuable information on the identification and determination of source
69 contributions. Nevertheless, the vertical variations and key drivers of formic acid,
70 particularly in urban regions, are still unclear due to the lack of adequate vertical
71 observations.

72 Isocyanic acid (HNCO) is an inorganic acid and has attracted extensive concerns
73 worldwide in recent years due to its strong toxicity (*Wang et al., 2007; Jaisson et al.,*
74 *2011; Koeth et al., 2013*). Previous studies have reported that isocyanic acid is highly
75 soluble at physiological pH and the dissociated cyanate ions (NCO^-) are closely linked
76 to atherosclerosis, cataracts, and rheumatoid arthritis (*Mydel et al., 2010; Roberts et al.,*
77 *2011*). At present, there is no standard to clearly define the critical levels of isocyanic
78 acid pollution in ambient air (*Rosanka et al., 2020*). A mixing ratio of 1 ppbv was
79 considered the upper limit of ambient isocyanic acid, which is derived from the
80 threshold of protein carbamylation reactions initiated by HNCO or NCO^- in human
81 body (*Verbrugge et al., 2015; Fulgham et al., 2020*). Similar to formic acid, our
82 understanding of isocyanic acid sources is also very limited.

83 As reported in the literature, primary emissions of isocyanic acid are mainly from
84 combustion sources including cigarette smoke (*Hems et al., 2019*), gasoline and diesel
85 engine exhausts (*Wren et al., 2018*), and biomass combustion (*Wentzell et al., 2013; Li*
86 *et al., 2021; Chandra and Sinha, 2016*). Wet and dry deposition is known as the main
87 sink of isocyanic acid (*Roberts et al., 2014; Rosanka et al., 2020*). In addition, isocyanic
88 acid is highly soluble at atmospheric pH and can be hydrolyzed to NH_3 and CO_2 (*Zhao*
89 *et al., 2014; Roberts and Liu, 2019*). Secondary formation is another important source
90 of atmospheric isocyanic acid and the known precursors include amides (*Barnes et al.,*
91 *2010*), urea (*Jathar et al., 2017*), and nicotine (*Roberts et al., 2011; Borduas et al.,*
92 *2016*).

93 Amides are reported to be the main precursors of isocyanic acid in urban region
94 (*Wang et al., 2020*). Isocyanic acid is the oxidative degradation product of amides
95 initiated by OH radicals, NO_3 radicals, and Cl atoms (*Barnes et al., 2010*). In addition



96 to primary emissions from organic solvents and various industrial processes, amides
97 can be also formed through the atmospheric accretion reactions of organic acids with
98 amines or ammonia (*Barnes et al., 2010; Yao et al., 2016*). The degradation of formic
99 acid may be an important formation pathway of isocyanic acid in the atmosphere. For
100 example, formamide could be formed from the atmospheric accretion reactions of
101 formic acid with amines or ammonia and then produce isocyanic acid through reactions
102 with OH radicals, NO₃ radicals, and Cl atoms. The vertical variations of formic acid
103 will also have vital impacts on the sources and vertical distributions of isocyanic acid
104 if the above-mentioned speculation is true. Unfortunately, the vertical distributions of
105 isocyanic acid are also poorly understood due to the lack of measurements.

106 Chemical ionization mass spectrometer (CIMS) can effectively detect and
107 quantify atmospheric formic and isocyanic acids (*Bannan et al., 2014; Chandra and*
108 *Sinha, 2016; Liggio et al., 2017; Mungall et al., 2018; Fulgham et al., 2019*). However,
109 the big mass, large volume, and strict operation environments of CIMS limit its wide
110 application in making vertical measurements of formic and isocyanic acids. CIMS has
111 been widely used onboard aircraft or on towers to make online vertical measurements
112 of formic and isocyanic acids (*Liggio et al., 2017; Mattila et al., 2018*). Aircraft can
113 carry many types of instruments and achieve measurements of a large suite of
114 parameters (*Benish et al., 2020; Zhao et al., 2021*), but the cost is also very expensive.
115 Towers can provide vertical observations of target species by setting up sites at different
116 heights, building mobile platforms (elevators or baskets) (*Mattila et al., 2018*), and
117 drawing air from multiple heights to the ground-based instruments through long tubes
118 (*Hu et al., 2013; Yáñez-Serrano et al., 2018*). The usage of long tubes is the most
119 convenient and cost-effective method to make gradient measurements of target gaseous
120 species so far. However, interactions between gaseous species and tubing walls may
121 bring unexpected uncertainties for their measurements (*Helmig et al., 2008a; Helmig*
122 *et al., 2008b; Schnitzhofer et al., 2009; Sweeney et al., 2010; Pagonis et al., 2017*).
123 Therefore, the impacts of long tubing on measurements of formic and isocyanic acids



124 need to be elucidated.

125 In this study, we first assessed the effects of long perfluoroalkoxy alkane (PFA)
126 Teflon tubes on measurements of formic and isocyanic acids. Vertical gradient
127 measurements of the two acids were made through long tubes on a tall tower in urban
128 Beijing, China. Then, the vertical variations and sources of the two acids were
129 investigated and discussed. At last, key conclusions and implications of this study were
130 summarized.

131 **2. Methods and materials**

132 **2.1. Site description and field campaign**

133 Vertical gradient measurements of gaseous species were made on the Beijing
134 Meteorological Tower, which is located on the campus of the Institute of Atmospheric
135 Physics (IAP), Chinese Academy of Sciences. Beijing is the capital city of China with
136 a population of over 20 million by 2020. Beijing has large anthropogenic emission
137 intensities and is suffering from severe air pollution problems (*Acton et al., 2020; Meng*
138 *et al., 2020; Tan et al., 2022*). The tower is located in the northern part of downtown
139 Beijing between the 3rd and 4th Ring Roads and is surrounded by urban roads,
140 expressways, residential areas, restaurants, urban landscaping, and parks. As a result,
141 concentrations of the primary pollutants at the tower site are mainly contributed by both
142 anthropogenic (e.g., vehicular exhausts, cooking, and household volatile chemical
143 products) and biogenic emissions. Detailed descriptions of the tower have been
144 provided in previous studies (*Acton et al., 2020; Yan et al., 2021*) and will not be
145 repeated here. The field campaign was carried out from July 17th to August 3rd, 2021.

146 **2.2. Instrumentation**

147 To obtain online gradient measurements of atmospheric trace gases, we
148 established a tower-based observation system using a combination of online
149 measurement techniques and long tubes. The system and related assessments on the



150 usage of long tubes have been explicitly described in our previous study (*Li et al., 2023*)
151 and will be briefly introduced here. After removing fine particles by PFA Teflon filters,
152 ambient air at four altitudes on the tower (namely 47, 102, 200, and 320 m) was
153 simultaneously and continuously drawn to the ground through long PFA Teflon tubes
154 (100, 150, 250, and 400 m; outer diameter: 1/2"; inner diameter: 0.374") by a pump.
155 The flow rate of the sample stream in each tube was controlled by a critical orifice and
156 ranged between 14-19 standard liters per minute (SLPM). The flow rates in long tubes
157 were retained as large as possible if instruments allowed to minimize the impact of gas-
158 surface interactions on measurements of targeted gaseous species (*Deming et al., 2019*;
159 *Li et al., 2023*). Two air-conditioned containers were placed next to each other on the
160 base of the tower and all the instruments were operated inside. An additional inlet of
161 the tube was mounted on the rooftop of the container (approximately 5 m above ground
162 level) to make measurements of trace gases near the surface. Therefore, the tower-based
163 observation system consisted of five inlet heights ranging from the ground level to 320
164 m. Inlets of the instruments were connected to the outlet of a Teflon solenoid valve
165 group, which was used to perform the switch of the inlet heights at time intervals of 4
166 minutes. Vertical gradient measurements of gaseous species were cyclically made over
167 periods of 20 minutes. Indoor PFA Teflon tubes were wrapped with insulation tubes and
168 were heated to prevent condensation of water and organic gases.

169 Formic and isocyanic acids were measured by a high-resolution time-of-flight
170 chemical ionization mass spectrometer with iodide reagent ion (ToF-CIMS). A Filter
171 Inlet for Gases and AEROSols (FIGAERO) was used to perform the switch between the
172 gas and particle measurement modes (*Lopez-Hilfiker et al., 2014*). The ionic molecular
173 reaction (IMR) chamber is adjacent to the FIGAERO and utilizes a vacuum ultraviolet
174 ion source (VUV-IS). Iodide anion (I^-) is produced from the photoionization of methyl
175 iodide (CH_3I) in MIR (*Ji et al., 2020*). During the measurements, I^- was produced by
176 introducing the CH_3I gas standard (1000 ppm, Dalian Special Gases, China) to the IMR
177 chamber at a flow rate of 2 standard cubic centimeters per minute (SCCM) in 200



178 SCCM high-purity nitrogen (N₂, 99.9995%) by the VUV-IS. The pressure of the IMR
179 chamber was maintained at 70-80 mbar. Due to the high sensitivity to oxygenated
180 volatile organic compounds (OVOCs), the iodine ion source has been widely used in
181 previous studies (*Yuan et al., 2015; Schobesberger et al., 2016; Mungall et al., 2018*).
182 Flow rates of the sample gas were maintained at 2 SLPM using a critical orifice. During
183 the field campaign, the FIGAERO was set to 24 minutes for gas measurements and 36
184 minutes for particle measurements in one-hour cycles. In gas mode, the first 21 minutes
185 were used to measure ambient air and the last 3 minutes were used for instrument
186 background measurements by introducing zero air at 3 SLPM. In addition, instrument
187 background measurements were also made for 10 s at time intervals of 210 s (*Palm et*
188 *al., 2019*).

189 Calibrations of the ToF-CIMS for formic and isocyanic acids were performed in
190 the laboratory before and after the field campaign. Standard solutions of formic acid
191 were evaporated using the liquid calibration unit (LCU, IONICON Analytik GmbH)
192 and then diluted to designated concentration gradients by being mixed with zero air at
193 five flow rates. The gas standard of isocyanic acid is unstable at ambient temperature
194 and thus no commercial gas cylinder was available. Instead, cyanuric acid solution was
195 put into a diffusion cell and heated to 300 °C to generate isocyanic acid gas at a stable
196 mixing ratio. An ion chromatograph was used to quantify the concentration of the gas
197 standard by measuring deionized water that absorbed the isocyanic acid gas. Detailed
198 information about the isocyanic acid calibration procedure has been provided in our
199 previous work (*Wang et al., 2020*). Impacts of the changes in ambient humidity on
200 measurements of the ToF-CIMS for both formic and isocyanic acids were determined
201 in the laboratory and were eliminated when calculating their respective concentrations.
202 Measured signals of the ToF-CIMS were processed using the Tofware software package
203 (version 3.0.3; Tofwerk AG, Switzerland).

204 A high time-resolution proton-transfer-reaction quadrupole interface time-of-
205 flight mass spectrometer (PTR-ToF-MS) with both H₃O⁺ and NO⁺ ion chemistry was



206 used to make some precursor measurements of the two acids, such as isoprene,
207 aromatics, OVOCs, and amides. Detailed information about the configuration and
208 operation setup of the PTR-ToF-MS has been provided in our previous studies (*Yuan et*
209 *al.*, 2017; *Wu et al.*, 2020; *Li et al.*, 2022). Mixing ratios of O₃, CO, and NO₂ were
210 measured by a UV absorption O₃ analyzer (T400, Teledyne API, USA), a gas filter
211 correlation CO analyzer (T300, Teledyne API, USA), and a trace level NO_x analyzer
212 (42i, Thermos, USA), respectively. Photolysis rates were measured by a PFS-100
213 photolysis spectrometer (Focused Photonics Inc.) on the rooftop of the container. The
214 planetary boundary layer height (PBLH) data was obtained from the website of the Air
215 Resources Laboratory (<https://ready.arl.noaa.gov/READYamet.php>). Measurements of
216 isocyanic acid and amides made in Guangzhou and Gucheng in China were also used
217 in this study for comparison, and more information about these observations can be
218 found in our previous papers (*Wang et al.*, 2020).

219 **2.3. Tubing assessment**

220 The tower-based observation system used long PFA Teflon tubes (hundreds of
221 meters in length) to draw air samples from different heights. The interactions between
222 tubing inner walls and organic compounds, namely the absorption/desorption of trace
223 gases, have nonnegligible impacts on their measurements after traversing such long
224 tubes (*Pagonis et al.*, 2017; *Deming et al.*, 2019). The equilibrium between the
225 absorption and desorption of organic compounds on tubing walls required distinct times,
226 namely tubing delay, for different species. For nonpolar/weak-polar organic compounds,
227 their tubing delays and measurement uncertainties after traversing long tubes are
228 dependent on their saturation concentrations and the flow rates of sample streams but
229 are independent of changes in humidity (*Krechmer et al.*, 2017; *Pagonis et al.*, 2017).
230 For some small polar organic compounds, their tubing delays and measurement
231 uncertainties after traversing long tubes are dependent on Henry's law coefficients and
232 are affected by changes in humidity (*Liu et al.*, 2019). The performance of long PFA
233 Teflon tubes in measuring concentrations of nonpolar/weak-polar organic compounds



234 and inorganic species (e.g., ozone, NO, NO₂, and CO₂) has been assessed in our
235 previous work (*Li et al., 2023*). The impacts of long PFA Teflon tubes on measurements
236 of formic and isocyanic acids are still unclear and will be assessed in this study.

237 Long PFA Teflon tubes with an outer diameter of 1/2" and an inner diameter of
238 0.374" were used to draw air samples from different altitudes and thus were assessed.
239 At flow rates below 20 SLPM, suitable pressure drops can be maintained in these long
240 tubes for instrument operation (*Li et al., 2023*). The effects of long tubes on
241 measurements of formic and isocyanic acids were mainly assessed using the same
242 methods in the literature (*Li et al., 2023*). The tubing delay of formic acid is estimated
243 as the time required to reach 90% of the concentration change made at the tubing inlet.
244 The depassivation curve of formic acid measured at the air outlet end of the tubing was
245 used to calculate its tubing delay and was obtained by using a step-function change in
246 its concentration at the tubing inlet (*Pagonis et al., 2017; Deming et al., 2019*). The
247 formic acid signals were normalized to those measured at the beginning of the step-
248 function change and then were fitted using the double exponential method, as shown in
249 Figure 1. Finally, the tubing delay of formic acid was determined when the fitting line
250 decreased to 0.1. The previous study (*Li et al., 2023*) has reported that inorganic species
251 have small tubing delays even in a 400 m long tube. Therefore, tubing delays of
252 isocyanic acid in long tubes are not discussed in this study.

253 To further assess the impacts of long tubes (namely 100, 200, 300, and 400 m)
254 on measurements of formic and isocyanic acids in real environments, their ambient
255 mixing ratios measured through different lengths of tubes were intercompared by
256 running the inlets side by side at ground level. Ambient air samples were sequentially
257 drawn with and without the tubes through a Teflon solenoid valve group (Figure S1),
258 which was set to perform the switch at time intervals of 4 minutes. Instrument
259 backgrounds of the two species were measured for 10 s at time intervals of 1 minute by
260 passing zero air into the instrument at a flow rate of 3 SLPM. Inter-comparisons of the
261 formic acid and isocyanic acid measurements made through different lengths of tubes



262 were mainly performed using linear fittings ($y=kx+b$; k is the slope and b is the
263 intercept).

264 **3. Results and Discussions**

265 **3.1. Interactions between long tubes and the two acids**

266 As shown in Figure 1, signals of formic acid measured by the ToF-CIMS had a
267 tubing delay of 23 s after traversing the 400 m long tube at the flow rate of 13 SLPM.
268 In addition to the interactions between tubing walls and formic acid molecules (*Pagonis*
269 *et al.*, 2017; *Deming et al.*, 2019), molecular diffusion and dispersion (namely Taylor
270 dispersion) can cause the longitudinal mixing of gas molecules in the tubing and is also
271 an important factor contributing to the measured delays (*Sweeney et al.*, 2010).
272 Molecular diffusion and dispersion have strong dependences on molecular diffusion
273 coefficients and tubing flow rates (*Karion et al.*, 2010). The influential time of Taylor
274 dispersion on the measurements of formic acid through a 400 m long tube at the flow
275 rate of 13 SLPM was estimated to be only 2.9 s, which is much smaller than the
276 measured tubing delay (23 s) of formic acid. Therefore, the adsorption/desorption of
277 formic acid molecules on tubing inner walls plays a dominant role in determining the
278 tubing delay.

279 For most organic compounds, the tubing delays generally depend on tubing flow
280 rates and their saturated concentrations (C^*) (*Li et al.*, 2023; *Deming et al.*, 2019). With
281 the increase in tubing length and flow rate, the tubing delays of organic compounds will
282 rapidly decrease (*Liu et al.*, 2019). Therefore, the tubing flow rates should be as large
283 as possible if the instrument could work normally. In addition, the tubing delays of
284 organic compounds generally increase with the decrease in their C^* (*Li et al.*, 2023). It
285 must be acknowledged that tubing delay is inevitable. The analysis time scales of
286 species concentrations measured through long tubes should be greater than their tubing
287 delays, especially for those with small C^* .

288 As shown in Figure S2(a), ambient mixing ratios of formic acid measured



289 through the 400 m long tube varied consistently with those measured without the tube
290 with mean values of 4.14 and 4.09 ppbv, respectively. The mixing ratios of formic acid
291 measured with the long tube were slightly higher in the daytime and lower at night in
292 comparison with those measured without the long tube. We also conducted a correlation
293 analysis between the mixing ratios of formic acid measured with and without long tubes.
294 As shown in Figure 2, the mixing ratios of formic acid measured with and without the
295 400 m long tube agreed within 20%, but the slope of the linear fitting ($k=0.84$) is lower
296 than 1. The differences of formic acid mixing ratios measured with and without the 400
297 m long tube were predominantly caused by the long-tail memory effect of the tubing
298 (Figure 1). For example, the mixing ratios of formic acid measured through the 400 m
299 long tube at night equaled to its ambient mixing ratios plus those released from the
300 tubing inner wall. The tubing delay of formic acid was determined when its mixing
301 ratios reached 90% of the change before entering the tubing. However, the long-tail
302 memory effect of the tubing mainly focused on the rest 10% of the change (Figure 1),
303 which required a much longer time to stabilize.

304 Impacts of the tubing memory effects will be accumulated due to the continuous
305 change in ambient concentrations of formic acid. To further assess the impacts of tubing
306 memory effects on measurement uncertainties of the two acids, differences between
307 mixing ratios of the species X (namely formic and isocyanic acids) measured with and
308 without long tubes at time t (denoted by $\delta[X]_t$) were calculated using Eq. (1):

$$309 \quad \delta[X]_t = [X_{without}]_t - [X_{with}]_t \quad (1)$$

310 where $[X_{with}]_t$ and $[X_{without}]_t$ refer to mixing ratios of the species X measured at
311 time t with and without long tubes, respectively; Δt is the change in time relative to
312 time t and was used to characterize the influential time of the memory effect. In addition,
313 the changes in mixing ratios of the species X measured using long tubes at time t relative
314 to its average mixing ratio over the previous time interval of Δt (denoted by $\Delta[X]_t$)
315 was also calculated using Eq. (2):

$$316 \quad \Delta[X]_t = [X_{with}]_t - \frac{\sum_{t-\Delta t}^t [X_{with}]}{\Delta t} \quad (2)$$



317 A strong correlation between $\delta[X]_t$ and $\Delta[X]_t$ could be captured at a certain Δt if
318 the tubing memory effect make essential contributions to measurement uncertainties of
319 the species X after traversing long tubes. For the 400 m long tubing, $\delta[X]_t$ and $\Delta[X]_t$
320 had the strongest correlation ($R^2=0.89$) when Δt was approximately 14 h (Figure S3).
321 As also shown in Figure 2(a), the mixing ratios of formic acid measured with and
322 without the 400 m long tube agreed well when $\Delta[HCOOH]$ approached to zero. The
323 decrease and increase in $\Delta[HCOOH]$ will enlarge measurement uncertainties of formic
324 acid using the long tube. In morning periods, ambient mixing ratios of formic acid
325 rapidly increased. As a result, the mixing ratios of formic acid measured through the
326 400 m long tube were slightly lower than its ambient mixing ratios due to the absorption
327 of formic acid by tubing inner walls. In evening and nighttime periods, an opposite
328 phenomenon was observed due to the desorption of formic acid from tubing inner walls
329 (Figure S2). In addition to the 400 m long tube, impacts of the tubes with lengths of
330 100, 200, and 300 m on measurements of formic acid were also assessed, as shown in
331 Figures 2(c) and 3(a). The usage of tubes with lengths of 100, 200, and 300 m has
332 negligible impacts on the measurements of formic acid.

333 In contrast to formic acid, the usage of long tubes had minor impacts on the
334 measurements of isocyanic acid. The mixing ratios of isocyanic acid measured with and
335 without the 400 m long tube varied consistently ($k=0.86$, $R^2=0.90$) with mean values of
336 0.25 and 0.26 ppbv, respectively (Figure S2). As shown in Figure 2(b), $\Delta[HNCO]$ is
337 evenly distributed on both sides of the 1:1 line. Therefore, the changes in ambient
338 concentrations of isocyanic acid do not have significant impacts on the measurements
339 of isocyanic acid through the long tubes. As also shown in Figure 3(b), $\delta[HNCO]$ and
340 $\Delta[HNCO]$ of isocyanic acid were independent of the changes in isocyanic acid mixing
341 ratios. The R^2 values of linear fittings were less than 0.21 for the isocyanic acid
342 measurements made using different lengths of tubes. This is consistent with the results
343 reported in the literature (Helmig *et al.*, 2008a; Helmig *et al.*, 2008b; Li *et al.*, 2023)
344 that inorganic species with low reactivities can be well measured using long PFA Teflon



345 tubes. The test results confirm that the measurements of formic and isocyanic acids
346 made through long tubes can be used to characterize their vertical and temporal
347 variations.

348 **3.2. Vertical variations and sources of formic acid**

349 Time series of formic acid and ozone mixing ratios at 5 and 320 m are shown in
350 Figure 4. The concentrations of formic acid and ozone exhibited similar diurnal and
351 inter-diurnal variations at different altitudes during the campaign. Hourly mean mixing
352 ratios of ozone exhibited strong temporal variations with an average of 43.5 ± 25.3 ppbv
353 at 5 m and an average of 53.5 ± 25.0 ppbv at 320 m. Hourly mean mixing ratios of formic
354 acid at 5 m ranged between 0.1–6.6 ppbv with an average of 1.3 ± 1.3 ppbv at 5 m, which
355 is comparable to those observed in other megacities, such as Shenzhen (1.2 ppbv) in
356 China (Zhu *et al.*, 2019), London (1.3 ppbv) in UK (Bannan *et al.*, 2017), and Los
357 Angeles (2.0 ppbv) in USA (Yuan *et al.*, 2015). By contrast, hourly mean mixing ratios
358 of formic acid at 320 m had an average of 2.1 ± 1.9 ppbv, approximately 1.6 times higher
359 than that at 5 m. The temporal variability of formic and isocyanic acids were mainly
360 caused by the diurnal and inter-diurnal changes in meteorological conditions (e.g., solar
361 radiation and PBLH).

362 Before July 12th, the daily maximum hourly mixing ratios of ozone at 5 m all
363 exceeded 100 ppbv, indicating the enhanced formation of secondary air pollutants
364 associated with photochemical reactions. The mixing ratios of formic acid measured
365 before July 12th were also prominently larger than those measured after, suggesting
366 important contributions from photochemical formations. Because of the precipitation,
367 weak solar radiation (characterized by small $j(\text{NO}_2)$ values) and small PBLHs were
368 observed from July 13th to 30th, largely suppressing the photochemical formation of
369 secondary air pollutants. After August 1st, low mixing ratios of ozone and formic acids
370 were observed along with the occurrence of favorable dilution conditions characterized
371 by high PBLHs.

372 As shown in Figure 5, the mixing ratios of formic acid measured at the five



373 altitudes (namely 5, 47, 102, 200, and 320 m) exhibited similar diurnal patterns. After
374 sunrise (~6:00 LT), formic acid mixing ratios increased rapidly at each altitude before
375 reaching the peak between 14:00-16:00 LT and then continuously declined before
376 sunrise the following day. Similar diurnal variation patterns of formic acid were also
377 observed at other urban sites (*Veres et al., 2011*), rural sites (*Hu et al., 2022*), and remote
378 sites (*Schobesberger et al., 2016*). The diurnal variation patterns of formic acid were
379 highly similar to those of ozone (a typical secondary pollutant) but were different from
380 those of VOCs from primary emissions. Taking toluene as an example, toluene is a
381 typical VOC tracer of anthropogenic emission sources in urban regions, such as
382 industrial processes and vehicular exhausts (*Fang et al., 2016; Skorokhod et al., 2017*),
383 and is also an important precursor of ozone (*Yuan et al., 2012*). The mixing ratios of
384 toluene exhibited opposite diurnal variation patterns to those of ozone and formic acids
385 with the minima occurring at around 14:00 LT. The lower mixing ratios of toluene in
386 daytime than in nighttime were predominantly caused by the enhancement of
387 atmospheric dilution and chemical removal by OH radicals (*De Gouw et al., 2018*). The
388 mixing ratios of formic acid poorly correlated (R^2 ranged between 0.16-0.28) with those
389 of CO (a typical tracer of combustion sources) at the five altitudes but well correlated
390 (R^2 ranged between 0.67-0.75) with those of Ox (O_3+NO_2 , a conserved metric of ozone
391 by removing NO titration effect), as shown in Figure 6. These results further confirm
392 that ambient concentrations of formic acid in urban Beijing were dominantly
393 contributed by secondary sources associated with photochemical reactions rather than
394 primary emissions.

395 Another observed evidence for the dominant contribution of formic acid from
396 secondary formations is its positive vertical gradients in nighttime (defined as the
397 period of 22:00-5:00 LT), as shown in Figure 7. Large amounts of formic acid will
398 accumulate near the surface with strong negative vertical gradients if primary emissions
399 dominate its contributions, as manifested by vertical toluene profiles. At nighttime, the
400 mixing ratios of ozone also increased with height due to enhanced removal by NO



401 titration and surface dry deposition. The deposition of formic acid was also enhanced
402 near the surface, driving the formation of positive gradients in vertical formic acid
403 profiles.

404 A notable difference existed between the diurnal variation patterns of ozone and
405 formic acid above the ground. As shown in Figure 5, the mean mixing ratios of ozone
406 at 5 m rapidly increased from 21.5 ppb to 36.0 ppb from 6:00 to 10:00 LT, while the
407 mean mixing ratios of ozone at 320 m slightly increased from 16.3 ppbv to 16.9 ppbv
408 during the same period. As shown in Figure 8, the growth rates of ozone mixing ratios
409 between 6:00 and 10:00 LT decreased with the increase in height. This phenomenon
410 indicates relatively weak photochemical ozone formation in urban regions aloft before
411 10:00 LT due to the lack of reactive ozone precursors (e.g., unsaturated hydrocarbons
412 and NO_x). With the enhancement of the vertical exchange of air masses with the rise of
413 the boundary layer, large amounts of ozone precursors (e.g., the observed peaks of
414 toluene mixing ratios at 320 m at 10:00 LT) emitted from surface sources were
415 transported upward and drove the formation of ozone in high altitudes. In contrast to
416 ozone, the mixing ratios of formic acid at the five altitudes all increased rapidly between
417 6:00 and 10:00 LT. The growth rate of formic acid mixing ratios between 6:00 and 10:00
418 LT kept nearly constant below 320 m (Figure 8). This result implies that the oxidation
419 products of VOCs over nighttime or in the daytime before are important precursors of
420 formic acid and can drive the rapid formation of formic acid with further photooxidation.
421 This speculation can be supported by the vertical and diurnal variations of methyl vinyl
422 ketone (MVK), methacrolein (MACR), and formaldehyde, which are reported key
423 precursors of formic acid as shown in Figure 5(d) and 5(e). The diurnal variation
424 patterns of MVK+MACR and formaldehyde at the five latitudes were nearly the same
425 with the enhancements in daytime. In addition, concentrations of MVK+MACR and
426 formaldehyde all increased with height in nighttime and early morning periods,
427 facilitating the photochemical formation of formic acid even in the residual layer.

428 As a reactive hydrocarbon species, the mixing ratios of toluene rapidly decreased



429 with height in daytime (defined as the period of 11:00-16:00 LT, as shown in Figure 7)
430 due to the combined effects of atmospheric dilution and OH-initiated chemical removal.
431 By contrast, the mixing ratios of ozone and formic acid increased with height. The
432 mixing ratios of ozone and formic acid all rapidly increased with height below 102 m,
433 predominantly attributed to the reduced effect of surface dry deposition with the
434 increase in height. The mean mixing ratios of formic acid increased by 18% from 102
435 m to 320 m in daytime, while ozone mixing ratios were well mixed above 102 m. These
436 observed results support the speculation that photochemical formations of formic acid
437 were substantially enhanced with the increase in height within the boundary layer.

438 The precursors and formation mechanisms of atmospheric formic acid have been
439 extensively investigated in previous studies but still remain uncertain. Isoprene has long
440 been recognized as an important precursor of formic acid through reactions with O₃ and
441 OH radicals (*Neeb et al., 1997; Paulot et al., 2009*). Recent studies also found that the
442 degradation of organic aerosols (OA) derived from isoprene is an important source of
443 formic acid (*Cope et al., 2021; Bates et al., 2023*). In addition, the photooxidation of
444 other biogenic and anthropogenic hydrocarbons is also a key source of formic acid
445 (*Paulot et al., 2011; Millet et al., 2015*). Figure 9 illustrates the mean vertical profiles
446 of several key precursors of formic acid in daytime. The concentrations of isoprene and
447 toluene (Figure 7) all decreased rapidly with height. By contrast, MVK and MACR, the
448 primary oxidation products of isoprene (*Grosjean et al., 1993*), exhibited weak vertical
449 gradients. Formaldehyde, a more general photooxidation product of VOCs, exhibited
450 similar vertical distribution patterns to those of ozone. Large amounts of OVOCs were
451 produced and accumulated in higher altitudes through the oxidation of hydrocarbons
452 and the further oxidation of some OVOCs during their upward mixing course. MVK,
453 MACR, and formaldehyde are also key precursors of formic acid. MVK and MACR
454 can react with O₃ to produce formic acid (*Link et al., 2020*). Formaldehyde can be
455 converted to methanediol in cloud droplets and then be rapidly oxidized by OH to
456 produce formic acid (*Franco et al., 2021*). In addition, enol (*Lei et al., 2020*) and many



457 other OVOCs (such as glycolaldehyde (*Butkovskaya et al., 2006a*) and hydroxyacetone
458 (*Butkovskaya et al., 2006b*) can be further oxidized to produce formic acid. Therefore,
459 high concentrations of OVOCs aloft may be the dominant factor that largely enhances
460 the photochemical formation of formic acid in urban regions.

461 As discussed above, formic acid exhibited strong positive vertical gradients
462 throughout the day, implying that the concentrations of formic acid measured at ground
463 level were not capable of accurately characterizing its abundance and temporal
464 variability in the whole boundary layer. Besides, the formic acid formed in daytime and
465 retained in the nocturnal residual layer also has vital impacts on the budget of formic
466 acid in the boundary layer. Thus, we used the column-integrated concentration (CIC)
467 of formic acid (the sum of the abundance in both the nocturnal residual layer and the
468 boundary layer, see detailed definitions in SI) to further clarify the diurnal variability
469 in the abundance of formic acid in the boundary layer.

470 As shown in Figure 4(f), the CICs of formic acid had a flatter diurnal pattern in
471 comparison to those at ground level. The CICs of formic acid had approximately stable
472 values overnight and reached a maximum at 16:00 LT. The ratio of the maximum and
473 minimum of CIC for formic acid was only 1.3, while it was 4.2 for the concentrations
474 of formic acid at 5 m. These results imply that the removal of atmospheric formic acid
475 (e.g., surface deposition and various chemical reactions) may be highly overestimated
476 if only ground-level measurements were used or constrained in numerical models. The
477 budget of the formic acid in high altitudes in the boundary layer was distinctly different
478 from those near the surface. As the result, numerical models cannot accurately
479 reproduce the abundances and budgets of formic acid without the constraints of vertical
480 observations and the clarification of formic acid formation mechanisms.

481 **3.3. Vertical variations and sources of isocyanic acid**

482 The mixing ratios of isocyanic acid also exhibited strong temporal variations
483 during the campaign with a mean of 0.28 ± 0.16 ppbv at 5 m and a mean of 0.43 ± 0.21
484 ppbv at 320 m, as shown in Figure 10. The mixing ratios of isocyanic acid measured at



485 the ground level in urban Beijing were approximately 10 times higher than those
486 measured in Los Angeles, USA (0.025 ppbv) (*Roberts et al., 2014*) and Calgary, Canada
487 (0.036 ppbv) (*Woodward-Massey et al., 2014*) but were lower than those measured in
488 other regions in China. For example, the mean mixing ratio of isocyanic acid was 0.37
489 ppbv at a rural site (Gucheng) in the North China Plain (NCP), and 0.46 ppbv in urban
490 Guangzhou in the Pearl River Delta (PRD) region (*Wang et al., 2020*). Isocyanic acid
491 will pose a threat to human health when its ambient mixing ratios exceed 1.0 ppbv. In
492 this study, isocyanic acid mixing ratios greater than 1.0 ppbv were not observed at
493 ground level but were observed at 320 m on three days. The maximum hourly mixing
494 ratios of isocyanic acid at 320 m reached 1.63 ppbv at 16:00 LT on July 8th.

495 The mixing ratios of isocyanic acid at the five altitudes exhibited similar diurnal
496 variation patterns. After sunrise, the mixing ratios of isocyanic acid at the five altitudes
497 all simultaneously increased and peaked at about 14:00 LT. Then, isocyanic acid mixing
498 ratios decreased slowly and reached the minimum before sunrise the following day.
499 This diurnal variation pattern of isocyanic acid measured at the ground level in urban
500 Beijing was not consistent with those measured at the Gucheng site in NCP (*Wang et*
501 *al., 2020*). The isocyanic acid mixing ratios at the Gucheng site exhibited insignificant
502 diurnal variability throughout the day with only a weak morning peak, predominantly
503 attributed to the enhancement of primary emissions. However, the diurnal variation
504 patterns of isocyanic acid measured at the five altitudes were well correlated with the
505 change in solar irradiance and were consistent with those measured at the two sites in
506 PRD. These results imply that ambient concentrations of isocyanic acid in urban Beijing
507 were mainly contributed by secondary sources associated with photochemical reactions.

508 Similar to formic acid, the simultaneous increase of isocyanic acid mixing ratios
509 at the five altitudes with the onset of sunlight also indicates the presence of adequate
510 precursors even in the nocturnal residual layer. In addition, the diurnal variability of
511 isocyanic acid mixing ratios measured below 200 m was much weaker than those
512 measured at 320 m. For example, the ratio of the daily maximum to the daily minimum



513 mixing ratios of isocyanic acid was 1.9 at 320 m, while the ratio was only 1.4 at 5 m.
514 The mean growth rate of isocyanic acid mixing ratios at 320 m (0.05 ppbv h^{-1}) between
515 6:00 and 10:00 LT was approximately five times larger than that at 5 m (0.01 ppbv h^{-1}).
516 The vertical gradients of isocyanic acid between 102 and 320 m were also larger than
517 those below (Figure 11). The rapid increase in both concentrations and growth rates of
518 isocyanic acid with height (Figures 8 and 11) implies the enhanced photochemical
519 formation of isocyanic acid in the middle and upper part of the boundary layer.

520 Secondary formation precursors of atmospheric isocyanic acid were still poorly
521 understood so far. Amides were considered important precursors of isocyanic acid
522 (Roberts *et al.*, 2014; Rosanka *et al.*, 2020). As reported in our previous study (Wang
523 *et al.*, 2020), C_3 amides accounted for the largest fraction of the total concentrations of
524 amides and were dominant contributors to the secondary formation of isocyanic acid.
525 The mixing ratios of C_3 amides in Guangzhou in PRD exhibited strong diurnal
526 variations. Along with the sunrise, the mixing ratios of C_3 amides rapidly decreased and
527 reached the minimum at 13:00 LT. Afterward, the mixing ratios of C_3 amides started to
528 increase and accumulated at night. However, the mixing ratios of C_3 amides in Beijing
529 and Gucheng in NCP exhibited insignificant diurnal variability, consistent with those
530 of isocyanic acid. The mean mixing ratios of C_3 amides at 5 m in urban Beijing is only
531 0.03 ppbv during the campaign, which is one order of magnitude lower than those in
532 Guangzhou (0.35 ppbv) and Gucheng (0.18 ppbv). The mixing ratios of C_3 amides
533 measured at the five altitudes in urban Beijing were also approximately one order of
534 magnitude lower than those of isocyanic acid (Figure 11). Besides, the mixing ratios of
535 C_3 amides decreased with height in both nighttime and daytime, indicating predominant
536 contributions from primary emissions. This is consistent with the fact that primary
537 emissions of chemical composition from industry-related sources have been largely
538 reduced with the outward migration of industry in urban Beijing. By contrast, the
539 mixing ratios of isocyanic acid increased with height in both day and night with an
540 average of 0.32 ppbv at 5 m and 0.60 ppbv at 320 m. These results suggest that C_3



541 amides were far more enough to account for the secondary formation of isocyanic acid
542 in urban Beijing.

543 Figure 12(a) gives the composition and average concentrations of C₁-C₁₀ amides
544 measured at the five altitudes during the campaign. C₂ amides accounted for the largest
545 fraction of the total mixing ratios of amides. The total mixing ratios of amides exhibited
546 decreasing tendencies with the increase in height, suggesting predominant contributions
547 from direct emissions of surface sources. As for formamide, its mixing ratios exhibited
548 an increasing tendency from 0.024 ppbv at 5 m to 0.030 ppbv at 320 m. The positive
549 vertical gradients of formamide suggest its enhanced formation with height, probably
550 due to the enhancements of formic acid. However, the average concentration ratios of
551 formamide to formic acid slightly varied between 0.01 and 0.02 among the five heights.
552 The average concentration ratios of formamide to isocyanic acid decreased from 0.09
553 at 5 m to 0.07 at 320 m. These results imply that the formation of isocyanic acid through
554 the pathway of HCOOH-CH₃NO-HNCO may be enhanced with the increase in height
555 but could only contribute a tiny fraction of the observed isocyanic acid, as shown in
556 Figure 12(b). Assuming the full conversion of C₁-C₁₀ amides to isocyanic acid, the
557 average concentration ratios of amides (sum of C₁-C₁₀) to isocyanic acid below 320 m
558 only ranged between 0.32 and 0.56 and decreased with height. Therefore, in addition to
559 amides, there must be other important precursors and formation pathways of isocyanic
560 acid, particularly in high altitudes. The simultaneous increase of isocyanic acid
561 concentrations at the five heights upon sunrise (Figure 10) implies the presence of
562 adequate precursors in the nocturnal residual layer. The oxidation products of VOCs
563 driven by ozone and NO₃ radicals in nighttime may be an important class of precursors.
564 In addition, the largest growth rates and highest concentrations of isocyanic acid at 320
565 m in daytime also suggest that high concentrations of OVOCs and low-NO_x conditions
566 may enhance the secondary formation of isocyanic acid.

567 The positive vertical gradients of isocyanic acid imply that the secondary
568 formation of isocyanic acid aloft could serve as an important source of surface isocyanic



569 acid in daytime driven by turbulence mixing. The CICs of isocyanic acid were
570 calculated to further clarify its abundance and temporal variability in the whole
571 boundary layer. Distinct diurnal patterns were observed between the ground-level
572 concentrations and CICs of isocyanic acid. Analogous to formic acid, the CICs of
573 isocyanic acid varied insignificantly over nighttime and enhanced in daytime, reaching
574 the maximum at approximately 14:00 LT. Therefore, the problems of formic acid
575 caused by the limitations of ground-level observations also raised for isocyanic acid.

576 **4. Conclusion**

577 In this study, vertical and diurnal variations of formic and isocyanic acids in
578 urban Beijing were investigated using tower-based online gradient measurements. The
579 measurements of isocyanic acid can be well measured through long PFA Teflon tubes.
580 The measurements of formic acid made through long tubes were slightly influenced by
581 the memory effect of tubing walls but had minor impacts on analyzing its vertical
582 distributions. The concentrations of formic and isocyanic acids all increased with height
583 in both nighttime and daytime. The diurnal and vertical distribution patterns of formic
584 and isocyanic acids all suggest that their abundances in the boundary layer were
585 dominantly contributed by secondary formation associated with photochemical
586 reactions. The photochemical formations of formic and isocyanic acids were also
587 substantially enhanced with the increase in height. The formation pathway of isocyanic
588 acid through $\text{HCOOH-CH}_3\text{NO-HNCO}$ only accounted for a tiny fraction of its ambient
589 abundance. The formic and isocyanic acids photochemically formed in the middle and
590 upper parts of the boundary layer were important sources for those at ground level in
591 urban region. The differences of the diurnal patterns between CICs and ground-level
592 concentrations of formic and isocyanic acids further highlight the importance of vertical
593 observations in elucidating their budgets and sources in the whole boundary layer.

594 Characterization of the vertical variations in formic and isocyanic acids could
595 provide valuable information for elucidating their budgets and sources in the boundary



596 layer. However, there are still many important but unresolved questions associated with
597 the vertical distributions of formic and isocyanic acids. For example, the key precursors
598 that drive the rapid formation of formic and isocyanic acids in the residual layer are still
599 unknown. Are there any changes in the key precursors and formation pathways of
600 formic and isocyanic acids with the increase of height in urban region? To answer these
601 questions, the combination of vertical gradient measurements of more chemical species
602 and numerical simulations is needed in future studies.

603 **Supporting Information:** Additional experimental details, materials, and methods,
604 including schematic illustration of tubing test, determination of the long tubes'
605 cumulative influence, and calculation of CICs..

606 **Data availability**

607 Data related to this article are available online
608 at <https://doi.org/10.7910/DVN/ANH0WE>.

609 **Author contributions**

610 QY, XBL, BY, and YH designed the research. QY, XBL, BY, XZ, YH, LY, XH,
611 JQ and MS contributed to the data collection and data analysis. QY and XBL wrote the
612 paper with contributions from all coauthors. All the coauthors discussed the results and
613 reviewed the paper.

614 **Competing interests**

615 The authors declare that they have no conflict of interest.

616 **Acknowledgment**

617 This work was financially supported by the National Key R&D Plan of China
618 (grant No. 2023YFC3706103, 2023YFC3706201, 2022YFC3700604) and the National
619 Natural Science Foundation of China (grant No. 42121004, 42275103, 42230701,
620 42305095). This work was also supported by the Special Fund Project for Science and



621 Technology Innovation Strategy of Guangdong Province (Grant No. 2019B121205004).
622 The authors would like to thank the personnel who participated in data collection,
623 instrument maintenance, and logistic support during the field campaign.

624 Reference

- 625 Acton, W. J. F., Huang, Z., Davison, B., Drysdale, W. S., Fu, P., Hollaway, M., Langford,
626 B., Lee, J., Liu, Y., Metzger, S., Mullinger, N., Nemitz, E., Reeves, C. E., Squires, F.
627 A., Vaughan, A. R., Wang, X., Wang, Z., Wild, O., Zhang, Q., Zhang, Y., and Hewitt,
628 C. N.: Surface-atmosphere fluxes of volatile organic compounds in Beijing,
629 Atmospheric Chemistry and Physics, 20, 15101-15125, 10.5194/acp-20-15101-2020,
630 2020.
- 631 Andreae, M. O., Talbot, R. W., Andreae, T. W., and Harriss, R. C.: Formic and acetic
632 acid over the central Amazon region, Brazil: 1. Dry season, 93, 1616-1624,
633 <https://doi.org/10.1029/JD093iD02p01616>, 1988.
- 634 Bannan, T. J., Bacak, A., Muller, J. B. A., Booth, A. M., Jones, B., Le Breton, M.,
635 Leather, K. E., Ghalaieny, M., Xiao, P., Shallcross, D. E., and Percival, C. J.:
636 Importance of direct anthropogenic emissions of formic acid measured by a chemical
637 ionisation mass spectrometer (CIMS) during the Winter ClearfLo Campaign in
638 London, January 2012, Atmospheric Environment, 83, 301-310,
639 10.1016/j.atmosenv.2013.10.029, 2014.
- 640 Bannan, T. J., Murray Booth, A., Le Breton, M., Bacak, A., Muller, J. B. A., Leather, K.
641 E., Khan, M. A. H., Lee, J. D., Dunmore, R. E., Hopkins, J. R., Fleming, Z. L., Sheps,
642 L., Taatjes, C. A., Shallcross, D. E., and Percival, C. J.: Seasonality of Formic Acid
643 (HCOOH) in London during the ClearfLo Campaign, Journal of Geophysical
644 Research: Atmospheres, 122, 10.1002/2017jd027064, 2017.
- 645 Barnes, I., Solignac, G., Mellouki, A., and Becker, K. H.: Aspects of the atmospheric
646 chemistry of amides, Chemphyschem, 11, 3844-3857, 10.1002/cphc.201000374,
647 2010.
- 648 Bates, K. H., Jacob, D. J., Cope, J. D., Chen, X., Millet, D. B., and Nguyen, T. B.:
649 Emerging investigator series: aqueous oxidation of isoprene-derived organic aerosol
650 species as a source of atmospheric formic and acetic acids, Environmental Science:
651 Atmospheres, 10.1039/d3ea00076a, 2023.
- 652 Benish, S. E., He, H., Ren, X., Roberts, S. J., Salawitch, R. J., Li, Z., Wang, F., Wang,
653 Y., Zhang, F., Shao, M., Lu, S., and Dickerson, R. R.: Measurement report: Aircraft
654 observations of ozone, nitrogen oxides, and volatile organic compounds over Hebei
655 Province, China, Atmospheric Chemistry and Physics, 20, 14523-14545,
656 10.5194/acp-20-14523-2020, 2020.
- 657 Borduas, N., Murphy, J. G., Wang, C., Silva, G. d., Abbatt, J. P. D. J. E. S., and Letters,
658 T.: Gas Phase Oxidation of Nicotine by OH Radicals: Kinetics, Mechanisms, and
659 Formation of HNCO, 3, 327-331, 2016.



- 660 Butkovskaya, N. I., Pouvesle, N., Kukui, A., and Le Bras, G.: Mechanism of the OH-
661 Initiated Oxidation of Glycolaldehyde over the Temperature Range 233–296 K, The
662 Journal of Physical Chemistry A, 110, 13492-13499, 10.1021/jp064993k, 2006a.
- 663 Butkovskaya, N. I., Pouvesle, N., Kukui, A., Mu, Y., and Le Bras, G.: Mechanism of
664 the OH-Initiated Oxidation of Hydroxyacetone over the Temperature Range 236–298
665 K, The Journal of Physical Chemistry A, 110, 6833-6843, 10.1021/jp056345r, 2006b.
- 666 Chandra, B. P. and Sinha, V.: Contribution of post-harvest agricultural paddy residue
667 fires in the N.W. Indo-Gangetic Plain to ambient carcinogenic benzenoids, toxic
668 isocyanic acid and carbon monoxide, Environ Int, 88, 187-197,
669 10.1016/j.envint.2015.12.025, 2016.
- 670 Chebbi, A. and Carlier, P.: Carboxylic acids in the troposphere, occurrence, sources,
671 and sinks: A review, Atmospheric Environment, 30, 4233-4249,
672 [https://doi.org/10.1016/1352-2310\(96\)00102-1](https://doi.org/10.1016/1352-2310(96)00102-1), 1996.
- 673 Cope, J. D., Abellar, K. A., Bates, K. H., Fu, X., and Nguyen, T. B.: Aqueous
674 Photochemistry of 2-Methyltetrol and Erythritol as Sources of Formic Acid and
675 Acetic Acid in the Atmosphere, ACS Earth and Space Chemistry, 5, 1265-1277,
676 10.1021/acsearthspacechem.1c00107, 2021.
- 677 de Gouw, J. A., Gilman, J. B., Kim, S. W., Alvarez, S. L., Dusanter, S., Graus, M.,
678 Griffith, S. M., Isaacman - VanWertz, G., Kuster, W. C., Lefer, B. L., Lerner, B. M.,
679 McDonald, B. C., Rappenglück, B., Roberts, J. M., Stevens, P. S., Stutz, J., Thalman,
680 R., Veres, P. R., Volkamer, R., Warneke, C., Washenfelder, R. A., and Young, C. J.:
681 Chemistry of Volatile Organic Compounds in the Los Angeles Basin: Formation of
682 Oxygenated Compounds and Determination of Emission Ratios, Journal of
683 Geophysical Research: Atmospheres, 123, 2298-2319, 10.1002/2017jd027976, 2018.
- 684 Deming, B. L., Pagonis, D., Liu, X., Day, D. A., Talukdar, R., Krechmer, J. E., de Gouw,
685 J. A., Jimenez, J. L., and Ziemann, P. J.: Measurements of delays of gas-phase
686 compounds in a wide variety of tubing materials due to gas-wall interactions,
687 Atmospheric Measurement Techniques, 12, 3453-3461, 10.5194/amt-12-3453-2019,
688 2019.
- 689 Enders, G., Dlugi, R., Steinbrecher, R., Clement, B., Daiber, R., Eijk, J. v., Gäb, S.,
690 Haziza, M., Helas, G., Herrmann, U., Kessel, M., Kesselmeier, J., Kotzias, D.,
691 Kourtidis, K., Kurth, H. H., McMillen, R. T., Roider, G., Schürmann, W., Teichmann,
692 U., and Torres, L.: Biosphere/Atmosphere interactions: Integrated research in a
693 European coniferous forest ecosystem, Atmospheric Environment. Part A. General
694 Topics, 26, 171-189, [https://doi.org/10.1016/0960-1686\(92\)90269-Q](https://doi.org/10.1016/0960-1686(92)90269-Q), 1992.
- 695 Fang, X., Shao, M., Stohl, A., Zhang, Q., Zheng, J., Guo, H., Wang, C., Wang, M., Ou,
696 J., Thompson, R. L., and Prinn, R. G.: Top-down estimates of benzene and toluene
697 emissions in the Pearl River Delta and Hong Kong, China, Atmospheric Chemistry
698 and Physics, 16, 3369-3382, 10.5194/acp-16-3369-2016, 2016.
- 699 Franco, B., Blumenstock, T., Cho, C., Clarisse, L., Clerbaux, C., Coheur, P. F., De
700 Mazière, M., De Smedt, I., Dorn, H. P., Emmerichs, T., Fuchs, H., Gkatzelis, G.,
701 Griffith, D. W. T., Gromov, S., Hannigan, J. W., Hase, F., Hohaus, T., Jones, N.,



- 702 Kerkweg, A., Kiendler-Scharr, A., Lutsch, E., Mahieu, E., Novelli, A., Ortega, I.,
703 Paton-Walsh, C., Pommier, M., Pozzer, A., Reimer, D., Rosanka, S., Sander, R.,
704 Schneider, M., Strong, K., Tillmann, R., Van Roozendaal, M., Vereecken, L.,
705 Vigouroux, C., Wahner, A., and Taraborrelli, D.: Ubiquitous atmospheric production
706 of organic acids mediated by cloud droplets, *Nature*, 593, 233-237, 10.1038/s41586-
707 021-03462-x, 2021.
- 708 Fulgham, S. R., Brophy, P., Link, M., Ortega, J., Pollack, I., and Farmer, D. K.: Seasonal
709 Flux Measurements over a Colorado Pine Forest Demonstrate a Persistent Source of
710 Organic Acids, *ACS Earth and Space Chemistry*, 3, 2017-2032,
711 10.1021/acsearthspacechem.9b00182, 2019.
- 712 Fulgham, S. R., Millet, D. B., Alwe, H. D., Goldstein, A. H., Schobesberger, S., and
713 Farmer, D. K.: Surface Wetness as an Unexpected Control on Forest Exchange of
714 Volatile Organic Acids, *Geophysical Research Letters*, 47, 10.1029/2020gl088745,
715 2020.
- 716 Galloway, J. N., Likens, G. E., Keene, W. C., and Miller, J. M.: The composition of
717 precipitation in remote areas of the world, 87, 8771-8786,
718 <https://doi.org/10.1029/JC087iC11p08771>, 1982.
- 719 Goode, J. G., Yokelson, R. J., Ward, D. E., Susott, R. A., Babbitt, R. E., Davies, M. A.,
720 and Hao, W. M.: Measurements of excess O₃, CO₂, CO, CH₄, C₂H₄, C₂H₂, HCN,
721 NO, NH₃, HCOOH, CH₃COOH, HCHO, and CH₃OH in 1997 Alaskan biomass
722 burning plumes by airborne Fourier transform infrared spectroscopy (AFTIR),
723 *Journal of Geophysical Research: Atmospheres*, 105, 22147-22166,
724 10.1029/2000jd900287, 2000.
- 725 Grosjean, D., Williams, E. L., II, and Grosjean, E.: Atmospheric chemistry of isoprene
726 and of its carbonyl products, *Environmental Science & Technology*, 27, 830-840,
727 10.1021/es00042a004, 1993.
- 728 Helmig, D., Johnson, B., Oltmans, S., Neff, W., Eisele, F., and Davis, D.: Elevated
729 ozone in the boundary layer at South Pole, *Atmospheric Environment*, 42, 2788-2803,
730 10.1016/j.atmosenv.2006.12.032, 2008a.
- 731 Helmig, D., Johnson, B., Warshawsky, M., Morse, T., Neff, W., Eisele, F., and Davis,
732 D.: Nitric oxide in the boundary-layer at South Pole during the Antarctic
733 Tropospheric Chemistry Investigation (ANTCI), *Atmospheric Environment*, 42,
734 2817-2830, 10.1016/j.atmosenv.2007.03.061, 2008b.
- 735 Hems, R. F., Wang, C., Collins, D. B., Zhou, S., Borduas-Dedekind, N., Siegel, J. A.,
736 and Abbatt, J. P. D.: Sources of isocyanic acid (HNCO) indoors: a focus on cigarette
737 smoke, *Environmental science. Processes & impacts*, 21, 1334-1341,
738 10.1039/c9em00107g, 2019.
- 739 Hu, L., Millet, D. B., Kim, S. Y., Wells, K. C., Griffis, T. J., Fischer, E. V., Helmig, D.,
740 Hueber, J., and Curtis, A. J.: North American acetone sources determined from tall
741 tower measurements and inverse modeling, *Atmos Chem Phys*, 13, 3379-3392,
742 10.5194/acp-13-3379-2013, 2013.
- 743 Hu, X., Yang, G., Liu, Y., Lu, Y., Wang, Y., Chen, H., Chen, J., and Wang, L.:



- 744 Atmospheric gaseous organic acids in winter in a rural site of the North China Plain,
745 Journal of Environmental Sciences, 113, 190-203, 10.1016/j.jes.2021.05.035, 2022.
- 746 Jacob, D. J.: Chemistry of OH in remote clouds and its role in the production of formic
747 acid and peroxymonosulfate, 91, 9807-9826,
748 <https://doi.org/10.1029/JD091iD09p09807>, 1986.
- 749 Jaisson, S., Pietrement, C., and Gillery, P.: Carbamylation-derived products: bioactive
750 compounds and potential biomarkers in chronic renal failure and atherosclerosis,
751 Clinical chemistry, 57, 1499-1505, 10.1373/clinchem.2011.163188, 2011.
- 752 Jathar, S. H., Heppding, C., Link, M. F., Farmer, D. K., Akherati, A., Kleeman, M. J.,
753 de Gouw, J. A., Veres, P. R., and Roberts, J. M.: Investigating diesel engines as an
754 atmospheric source of isocyanic acid in urban areas, Atmospheric Chemistry and
755 Physics, 17, 8959-8970, 10.5194/acp-17-8959-2017, 2017.
- 756 Ji, Y., Huey, L. G., Tanner, D. J., Lee, Y. R., Veres, P. R., Neuman, J. A., Wang, Y., and
757 Wang, X.: A vacuum ultraviolet ion source (VUV-IS) for iodide-chemical ionization
758 mass spectrometry: a substitute for radioactive ion sources, Atmospheric
759 Measurement Techniques, 13, 3683-3696, 10.5194/amt-13-3683-2020, 2020.
- 760 Karion, A., Sweeney, C., Tans, P., and Newberger, T.: AirCore: An Innovative
761 Atmospheric Sampling System, Journal of Atmospheric and Oceanic Technology, 27,
762 1839-1853, 10.1175/2010jtecha1448.1, 2010.
- 763 Kawamura, K. and Kaplan, I. R.: Organic compounds in the rainwater of Los Angeles,
764 Environ Sci Technol, 17, 497-501, 10.1021/es00114a011, 1983.
- 765 Kawamura, K., Steinberg, S., and Kaplan, I. R.: Homologous series of C1-C10
766 monocarboxylic acids and C1-C6 carbonyls in Los Angeles air and motor vehicle
767 exhausts, Atmospheric Environment, 34, 4175-4191, [https://doi.org/10.1016/S1352-](https://doi.org/10.1016/S1352-2310(00)00212-0)
768 [2310\(00\)00212-0](https://doi.org/10.1016/S1352-2310(00)00212-0), 2000.
- 769 Keene, W. C. and Galloway, J. N.: Organic acidity in precipitation of North America,
770 Atmospheric Environment (1967), 18, 2491-2497, [https://doi.org/10.1016/0004-](https://doi.org/10.1016/0004-6981(84)90020-9)
771 [6981\(84\)90020-9](https://doi.org/10.1016/0004-6981(84)90020-9), 1984.
- 772 Kesselmeier, J., Bode, K., Gerlach, C., and Jork, E. M.: Exchange of atmospheric
773 formic and acetic acids with trees and crop plants under controlled chamber and
774 purified air conditions, Atmospheric Environment, 32, 1765-1775,
775 [https://doi.org/10.1016/S1352-2310\(97\)00465-2](https://doi.org/10.1016/S1352-2310(97)00465-2), 1998.
- 776 Khare, P., Kumar, N., Kumari, K. M., and Srivastava, S. S.: Atmospheric formic and
777 acetic acids: An overview, 37, 227-248, <https://doi.org/10.1029/1998RG900005>,
778 1999.
- 779 Koeth, R. A., Kalantar-Zadeh, K., Wang, Z., Fu, X., Tang, W. H., and Hazen, S. L.:
780 Protein carbamylation predicts mortality in ESRD, J Am Soc Nephrol, 24, 853-861,
781 10.1681/ASN.2012030254, 2013.
- 782 Krechmer, J. E., Day, D. A., Ziemann, P. J., and Jimenez, J. L.: Direct Measurements
783 of Gas/Particle Partitioning and Mass Accommodation Coefficients in
784 Environmental Chambers, Environmental science & technology, 51, 11867-11875,
785 10.1021/acs.est.7b02144, 2017.



- 786 Le Breton, M., Bacak, A., Muller, J. B. A., Xiao, P., Shallcross, B. M. A., Batt, R.,
787 Cooke, M. C., Shallcross, D. E., Bauguitte, S. J. B., and Percival, C. J.: Simultaneous
788 airborne nitric acid and formic acid measurements using a chemical ionization mass
789 spectrometer around the UK: Analysis of primary and secondary production
790 pathways, *Atmospheric Environment*, 83, 166-175, 10.1016/j.atmosenv.2013.10.008,
791 2014.
- 792 Lei, X., Wang, W., Gao, J., Wang, S., and Wang, W.: Atmospheric Chemistry of Enols:
793 The Formation Mechanisms of Formic and Peroxyformic Acids in Ozonolysis of
794 Vinyl Alcohol, *J Phys Chem A*, 124, 4271-4279, 10.1021/acs.jpca.0c01480, 2020.
- 795 Li, T., Wang, Z., Yuan, B., Ye, C., Lin, Y., Wang, S., Sha, Q. e., Yuan, Z., Zheng, J., and
796 Shao, M.: Emissions of carboxylic acids, hydrogen cyanide (HCN) and isocyanic
797 acid (HNCO) from vehicle exhaust, *Atmospheric Environment*, 247,
798 10.1016/j.atmosenv.2021.118218, 2021.
- 799 Li, X.-B., Yuan, B., Wang, S., Wang, C., Lan, J., Liu, Z., Song, Y., He, X., Huangfu, Y.,
800 Pei, C., Cheng, P., Yang, S., Qi, J., Wu, C., Huang, S., You, Y., Chang, M., Zheng, H.,
801 Yang, W., Wang, X., and Shao, M.: Variations and sources of volatile organic
802 compounds (VOCs) in urban region: insights from measurements on a tall tower,
803 *Atmospheric Chemistry and Physics*, 22, 10567-10587, 10.5194/acp-22-10567-2022,
804 2022.
- 805 Li, X., Zhang, C., Liu, A., Yuan, B., Yang, H., Liu, C., Wang, S., Huangfu, Y., Qi, J.,
806 Liu, Z., He, X., Song, X., Chen, Y., Peng, Y., Zhang, X., Zheng, E., Yang, L., Yang,
807 Q., Qin, G., Zhou, J., and Shao, M.: Emerging investigator series: Assessment of
808 Long Tubing in Measuring Atmospheric Trace Gases: Applications on Tall Towers,
809 *Environmental Science: Atmospheres*, 10.1039/d2ea00110a, 2023.
- 810 Liggio, J., Moussa, S. G., Wentzell, J., Darlington, A., Liu, P., Leithead, A., Hayden, K.,
811 O'Brien, J., Mittermeier, R. L., Staebler, R., Wolde, M., and Li, S.-M.: Understanding
812 the primary emissions and secondary formation of gaseous organic acids in the oil
813 sands region of Alberta, Canada, *Atmospheric Chemistry and Physics*, 17, 8411-8427,
814 10.5194/acp-17-8411-2017, 2017.
- 815 Link, M. F., Nguyen, T. B., Bates, K., Müller, J.-F., and Farmer, D. K.: Can Isoprene
816 Oxidation Explain High Concentrations of Atmospheric Formic and Acetic Acid over
817 Forests?, *ACS Earth and Space Chemistry*, 4, 730-740,
818 10.1021/acsearthspacechem.0c00010, 2020.
- 819 Liu, X., Deming, B., Pagonis, D., Day, D. A., Palm, B. B., Talukdar, R., Roberts, J. M.,
820 Veres, P. R., Krechmer, J. E., Thornton, J. A., de Gouw, J. A., Ziemann, P. J., and
821 Jimenez, J. L.: Effects of gas-wall interactions on measurements of semivolatile
822 compounds and small polar molecules, *Atmospheric Measurement Techniques*, 12,
823 3137-3149, 10.5194/amt-12-3137-2019, 2019.
- 824 Lopez-Hilfiker, F. D., Mohr, C., Ehn, M., Rubach, F., Kleist, E., Wildt, J., Mentel, T. F.,
825 Lutz, A., Hallquist, M., Worsnop, D., and Thornton, J. A.: A novel method for online
826 analysis of gas and particle composition: description and evaluation of a Filter Inlet
827 for Gases and AEROsols (FIGAERO), *Atmos. Meas. Tech.*, 7, 983-1001,



- 828 10.5194/amt-7-983-2014, 2014.
- 829 Mattila, J. M., Brophy, P., Kirkland, J., Hall, S., Ullmann, K., Fischer, E. V., Brown, S.,
830 McDuffie, E., Tevlin, A., and Farmer, D. K.: Tropospheric sources and sinks of gas-
831 phase acids in the Colorado Front Range, *Atmospheric Chemistry and Physics*, 18,
832 12315-12327, 10.5194/acp-18-12315-2018, 2018.
- 833 Meng, F., Qin, M., Tang, K., Duan, J., Fang, W., Liang, S., Ye, K., Xie, P., Sun, Y., Xie,
834 C., Ye, C., Fu, P., Liu, J., and Liu, W.: High-resolution vertical distribution and
835 sources of HONO and NO₂ in the nocturnal boundary layer
836 in urban Beijing, China, *Atmospheric Chemistry and Physics*, 20, 5071-5092,
837 10.5194/acp-20-5071-2020, 2020.
- 838 Millet, D. B., Baasandorj, M., Farmer, D. K., Thornton, J. A., Baumann, K., Brophy, P.,
839 Chaliyakunnel, S., de Gouw, J. A., Graus, M., Hu, L., Koss, A., Lee, B. H., Lopez-
840 Hilfiker, F. D., Neuman, J. A., Paulot, F., Peischl, J., Pollack, I. B., Ryerson, T. B.,
841 Warneke, C., Williams, B. J., and Xu, J.: A large and ubiquitous source of
842 atmospheric formic acid, *Atmospheric Chemistry and Physics*, 15, 6283-6304,
843 10.5194/acp-15-6283-2015, 2015.
- 844 Mungall, E. L., Abbatt, J. P. D., Wentzell, J. J. B., Wentworth, G. R., Murphy, J. G.,
845 Kunkel, D., Gute, E., Tarasick, D. W., Sharma, S., Cox, C. J., Uttal, T., and Liggio,
846 J.: High gas-phase mixing ratios of formic and acetic acid in the High Arctic,
847 *Atmospheric Chemistry and Physics*, 18, 10237-10254, 10.5194/acp-18-10237-2018,
848 2018.
- 849 Mydel, P., Wang, Z., Brisslert, M., Hellvard, A., Dahlberg, L. E., Hazen, S. L., and
850 Bokarewa, M. I. J. T. J. o. I.: Carbamylation-Dependent Activation of T Cells: A
851 Novel Mechanism in the Pathogenesis of Autoimmune Arthritis, 184, 6882 - 6890,
852 2010.
- 853 Neeb, P., Sauer, F., Horie, O., and Moortgat, G. K.: Formation of hydroxymethyl
854 hydroperoxide and formic acid in alkene ozonolysis in the presence of water vapour,
855 *Atmospheric Environment*, 31, 1417-1423, [https://doi.org/10.1016/S1352-
856 2310\(96\)00322-6](https://doi.org/10.1016/S1352-2310(96)00322-6), 1997.
- 857 Pagonis, D., Krechmer, J. E., de Gouw, J., Jimenez, J. L., and Ziemann, P. J.: Effects of
858 gas-wall partitioning in Teflon tubing and instrumentation on time-resolved
859 measurements of gas-phase organic compounds, *Atmospheric Measurement
860 Techniques*, 10, 4687-4696, 10.5194/amt-10-4687-2017, 2017.
- 861 Palm, B. B., Liu, X., Jimenez, J. L., and Thornton, J. A.: Performance of a new coaxial
862 ion-molecule reaction region for low-pressure chemical ionization mass
863 spectrometry with reduced instrument wall interactions, *Atmospheric Measurement
864 Techniques*, 12, 5829-5844, 10.5194/amt-12-5829-2019, 2019.
- 865 Paulot, F., Crouse, J. D., Kjaergaard, H. G., Kroll, J. H., Seinfeld, J. H., and Wennberg,
866 P. O.: Isoprene photooxidation: new insights into the production of acids and organic
867 nitrates, *Atmos. Chem. Phys.*, 9, 1479-1501, 10.5194/acp-9-1479-2009, 2009.
- 868 Paulot, F., Wunch, D., Crouse, J. D., Toon, G. C., Millet, D. B., DeCarlo, P. F.,
869 Vigouroux, C., Deutscher, N. M., Gonzalez Abad, G., Notholt, J., Warneke, T.,



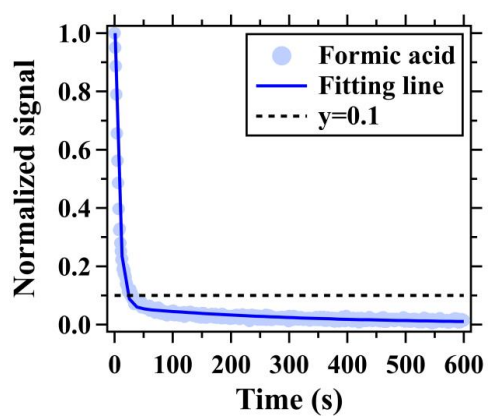
- 870 Hannigan, J. W., Warneke, C., de Gouw, J. A., Dunlea, E. J., De Maziere, M., Griffith,
871 D. W. T., Bernath, P., Jimenez, J. L., and Wennberg, P. O.: Importance of secondary
872 sources in the atmospheric budgets of formic and acetic acids, *Atmos Chem Phys*,
873 11, 1989-2013, 10.5194/acp-11-1989-2011, 2011.
- 874 Roberts, J. M. and Liu, Y.: Solubility and solution-phase chemistry of isocyanic acid,
875 methyl isocyanate, and cyanogen halides, *Atmospheric Chemistry and Physics*, 19,
876 4419-4437, 10.5194/acp-19-4419-2019, 2019.
- 877 Roberts, J. M., Veres, P. R., Cochran, A. K., Warneke, C., Burling, I. R., Yokelson, R.
878 J., Lerner, B., Gilman, J. B., Kuster, W. C., Fall, R., and de Gouw, J.: Isocyanic acid
879 in the atmosphere and its possible link to smoke-related health effects, *Proceedings*
880 *of the National Academy of Sciences of the United States of America*, 108, 8966-
881 8971, 10.1073/pnas.1103352108, 2011.
- 882 Roberts, J. M., Veres, P. R., VandenBoer, T. C., Warneke, C., Graus, M., Williams, E.
883 J., Lefer, B., Brock, C. A., Bahreini, R., Öztürk, F., Middlebrook, A. M., Wagner, N.
884 L., Dubé, W. P., and de Gouw, J. A.: New insights into atmospheric sources and sinks
885 of isocyanic acid, HNCO, from recent urban and regional observations, *Journal of*
886 *Geophysical Research: Atmospheres*, 119, 1060-1072, 10.1002/2013jd019931, 2014.
- 887 Rosanka, S., Vu, G. H. T., Nguyen, H. M. T., Pham, T. V., Javed, U., Taraborrelli, D.,
888 and Vereecken, L.: Atmospheric chemical loss processes of isocyanic acid (HNCO):
889 a combined theoretical kinetic and global modelling study, *Atmospheric Chemistry*
890 *and Physics*, 20, 6671-6686, 10.5194/acp-20-6671-2020, 2020.
- 891 Schnitzhofer, R., Wisthaler, A., and Hansel, A.: Real-time profiling of organic trace
892 gases in the planetary boundary layer by PTR-MS using a tethered balloon, *Atmos.*
893 *Meas. Tech.*, 2, 773-777, 10.5194/amt-2-773-2009, 2009.
- 894 Schobesberger, S., Lopez - Hilfiker, F. D., Taipale, D., Millet, D. B., D'Ambro, E. L.,
895 Rantala, P., Mammarella, I., Zhou, P., Wolfe, G. M., Lee, B. H., Boy, M., and
896 Thornton, J. A.: High upward fluxes of formic acid from a boreal forest canopy,
897 *Geophysical Research Letters*, 43, 9342-9351, 10.1002/2016gl069599, 2016.
- 898 Skorokhod, A. I., Berezina, E. V., Moiseenko, K. B., Elansky, N. F., and Belikov, I. B.:
899 Benzene and toluene in the surface air of northern Eurasia from TROICA-12
900 campaign along the Trans-Siberian Railway, *Atmospheric Chemistry and Physics*, 17,
901 5501-5514, 10.5194/acp-17-5501-2017, 2017.
- 902 Stavrakou, T., Müller, J. F., Peeters, J., Razavi, A., Clarisse, L., Clerbaux, C., Coheur,
903 P. F., Hurtmans, D., De Mazière, M., Vigouroux, C., Deutscher, N. M., Griffith, D.
904 W. T., Jones, N., and Paton-Walsh, C.: Satellite evidence for a large source of formic
905 acid from boreal and tropical forests, *Nature Geoscience*, 5, 26-30,
906 10.1038/ngeo1354, 2011.
- 907 Sweeney, C., Karion, A., Tans, P., and Newberger, T.: AirCore: An Innovative
908 Atmospheric Sampling System, *Journal of Atmospheric and Oceanic Technology*, 27,
909 1839-1853, 10.1175/2010jtecha1448.1, 2010.
- 910 Tan, Q., Ge, B., Xu, X., Gan, L., Yang, W., Chen, X., Pan, X., Wang, W., Li, J., and
911 Wang, Z.: Increasing impacts of the relative contributions of regional transport on air



- 912 pollution in Beijing: Observational evidence, *Environ Pollut*, 292, 118407,
913 10.1016/j.envpol.2021.118407, 2022.
- 914 Verbrugge, F. H., Tang, W. H., and Hazen, S. L.: Protein carbamylation and
915 cardiovascular disease, *Kidney Int*, 88, 474-478, 10.1038/ki.2015.166, 2015.
- 916 Veres, P. R., Roberts, J. M., Cochran, A. K., Gilman, J. B., Kuster, W. C., Holloway, J.
917 S., Graus, M., Flynn, J., Lefer, B., Warneke, C., and de Gouw, J.: Evidence of rapid
918 production of organic acids in an urban air mass, *Geophysical Research Letters*, 38,
919 n/a-n/a, 10.1029/2011gl048420, 2011.
- 920 Wang, Z., Nicholls, S. J., Rodriguez, E. R., Kummu, O., Horkko, S., Barnard, J.,
921 Reynolds, W. F., Topol, E. J., DiDonato, J. A., and Hazen, S. L.: Protein
922 carbamylation links inflammation, smoking, uremia and atherogenesis, *Nat Med*, 13,
923 1176-1184, 10.1038/nm1637, 2007.
- 924 Wang, Z., Yuan, B., Ye, C., Roberts, J., Wisthaler, A., Lin, Y., Li, T., Wu, C., Peng, Y.,
925 Wang, C., Wang, S., Yang, S., Wang, B., Qi, J., Wang, C., Song, W., Hu, W., Wang,
926 X., Xu, W., Ma, N., Kuang, Y., Tao, J., Zhang, Z., Su, H., Cheng, Y., Wang, X., and
927 Shao, M.: High Concentrations of Atmospheric Isocyanic Acid (HNCO) Produced
928 from Secondary Sources in China, *Environ Sci Technol*, 54, 11818-11826,
929 10.1021/acs.est.0c02843, 2020.
- 930 Wentzell, J. J., Liggio, J., Li, S. M., Vlasenko, A., Staebler, R., Lu, G., Poitras, M. J.,
931 Chan, T., and Brook, J. R.: Measurements of gas phase acids in diesel exhaust: a
932 relevant source of HNCO?, *Environ Sci Technol*, 47, 7663-7671, 10.1021/es401127j,
933 2013.
- 934 Woodward-Massey, R., Taha, Y. M., Moussa, S. G., and Osthoff, H. D.: Comparison of
935 negative-ion proton-transfer with iodide ion chemical ionization mass spectrometry
936 for quantification of isocyanic acid in ambient air, *Atmospheric Environment*, 98,
937 693-703, 10.1016/j.atmosenv.2014.09.014, 2014.
- 938 Wren, S. N., Liggio, J., Han, Y., Hayden, K., Lu, G., Mihele, C. M., Mittermeier, R. L.,
939 Stroud, C., Wentzell, J. J. B., and Brook, J. R.: Elucidating real-world vehicle
940 emission factors from mobile measurements over a large metropolitan region: a focus
941 on isocyanic acid, hydrogen cyanide, and black carbon, *Atmospheric Chemistry and
942 Physics*, 18, 16979-17001, 10.5194/acp-18-16979-2018, 2018.
- 943 Wu, C., Wang, C., Wang, S., Wang, W., Yuan, B., Qi, J., Wang, B., Wang, H., Wang, C.,
944 Song, W., Wang, X., Hu, W., Lou, S., Ye, C., Peng, Y., Wang, Z., Huangfu, Y., Xie,
945 Y., Zhu, M., Zheng, J., Wang, X., Jiang, B., Zhang, Z., and Shao, M.: Measurement
946 report: Important contributions of oxygenated compounds to emissions and
947 chemistry of volatile organic compounds in urban air, *Atmos. Chem. Phys.*, 20,
948 14769-14785, <https://doi.org/10.5194/acp-20-14769-2020>, 2020.
- 949 Yan, Y., Wang, S., Zhu, J., Guo, Y., Tang, G., Liu, B., An, X., Wang, Y., and Zhou, B.:
950 Vertically increased NO₃ radical in the nocturnal boundary layer, *Science of The
951 Total Environment*, 763, 142969, <https://doi.org/10.1016/j.scitotenv.2020.142969>,
952 2021.
- 953 Yáñez-Serrano, A. M., Nölscher, A. C., Bourtsoukidis, E., Gomes Alves, E., Ganzeveld,

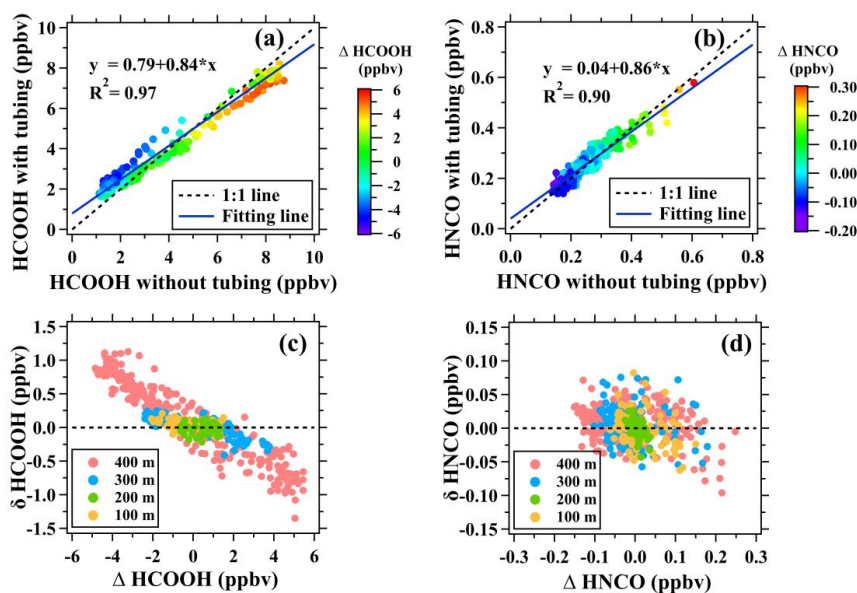


- 954 L., Bonn, B., Wolff, S., Sa, M., Yamasoe, M., Williams, J., Andreae, M. O., and
955 Kesselmeier, J.: Monoterpene chemical speciation in a tropical rainforest: variation
956 with season, height, and time of day at the Amazon Tall Tower Observatory (ATTO),
957 Atmospheric Chemistry and Physics, 18, 3403-3418, 10.5194/acp-18-3403-2018,
958 2018.
- 959 Yao, L., Wang, M. Y., Wang, X. K., Liu, Y. J., Chen, H. F., Zheng, J., Nie, W., Ding, A.
960 J., Geng, F. H., Wang, D. F., Chen, J. M., Worsnop, D. R., and Wang, L.: Detection
961 of atmospheric gaseous amines and amides by a high-resolution time-of-flight
962 chemical ionization mass spectrometer with protonated ethanol reagent ions, Atmos.
963 Chem. Phys., 16, 14527-14543, 10.5194/acp-16-14527-2016, 2016.
- 964 Yu, S.: Role of organic acids (formic, acetic, pyruvic and oxalic) in the formation of
965 cloud condensation nuclei (CCN): a review, Atmospheric Research, 53, 185-217,
966 [https://doi.org/10.1016/S0169-8095\(00\)00037-5](https://doi.org/10.1016/S0169-8095(00)00037-5), 2000.
- 967 Yuan, B., Koss, A. R., Warneke, C., Coggon, M., Sekimoto, K., and de Gouw, J. A.:
968 Proton-Transfer-Reaction Mass Spectrometry: Applications in Atmospheric Sciences,
969 Chem Rev, 117, 13187-13229, 10.1021/acs.chemrev.7b00325, 2017.
- 970 Yuan, B., Shao, M., de Gouw, J., Parrish, D. D., Lu, S., Wang, M., Zeng, L., Zhang, Q.,
971 Song, Y., Zhang, J., and Hu, M.: Volatile organic compounds (VOCs) in urban air:
972 How chemistry affects the interpretation of positive matrix factorization (PMF)
973 analysis, Journal of Geophysical Research: Atmospheres, 117, n/a-n/a,
974 10.1029/2012jd018236, 2012.
- 975 Yuan, B., Veres, P. R., Warneke, C., Roberts, J. M., Gilman, J. B., Koss, A., Edwards,
976 P. M., Graus, M., Kuster, W. C., Li, S. M., Wild, R. J., Brown, S. S., Dubé, W. P.,
977 Lerner, B. M., Williams, E. J., Johnson, J. E., Quinn, P. K., Bates, T. S., Lefer, B.,
978 Hayes, P. L., Jimenez, J. L., Weber, R. J., Zamora, R., Ervens, B., Millet, D. B.,
979 Rappenglück, B., and de Gouw, J. A.: Investigation of secondary formation of formic
980 acid: urban environment vs. oil and gas producing region, Atmospheric Chemistry
981 and Physics, 15, 1975-1993, 10.5194/acp-15-1975-2015, 2015.
- 982 Zhao, R., Yin, B., Zhang, N., Wang, J., Geng, C., Wang, X., Han, B., Li, K., Li, P., Yu,
983 H., Yang, W., and Bai, Z.: Aircraft-based observation of gaseous pollutants in the
984 lower troposphere over the Beijing-Tianjin-Hebei region, Sci Total Environ, 773,
985 144818, 10.1016/j.scitotenv.2020.144818, 2021.
- 986 Zhao, R., Lee, A. K. Y., Wentzell, J. J. B., McDonald, A. M., Toom-Sauntry, D., Leaitch,
987 W. R., Modini, R. L., Corrigan, A. L., Russell, L. M., Noone, K. J., Schroder, J. C.,
988 Bertram, A. K., Hawkins, L. N., Abbatt, J. P. D., and Liggio, J.: Cloud partitioning
989 of isocyanic acid (HNCO) and evidence of secondary source of HNCO in ambient
990 air, Geophysical Research Letters, 41, 6962-6969, 10.1002/2014gl061112, 2014.
- 991 Zhu, B., Han, Y., Wang, C., Huang, X., Xia, S., Niu, Y., Yin, Z., and He, L.:
992 Understanding primary and secondary sources of ambient oxygenated volatile
993 organic compounds in Shenzhen utilizing photochemical age-based parameterization
994 method, J Environ Sci (China), 75, 105-114, 10.1016/j.jes.2018.03.008, 2019.
- 995



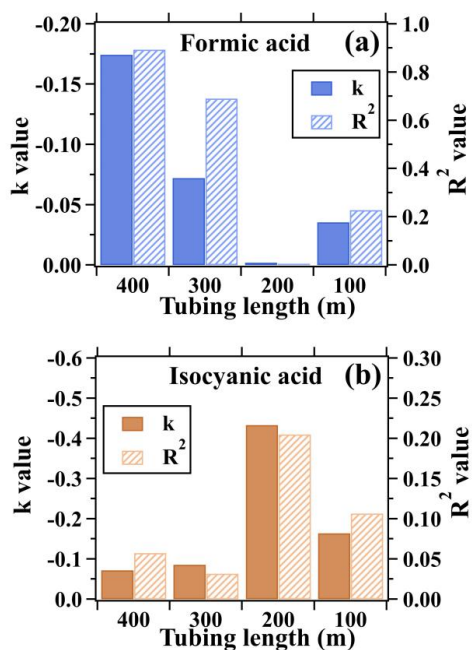
996

997 **Figure 1.** Depassivation curves of formic acid signal measured by I⁻ ToF-CIMS for the
998 400 m long tubing at the flow rate of 13 SLPM. Ion signals were normalized to those
999 measured at the start time (0 s) of the step-function change.



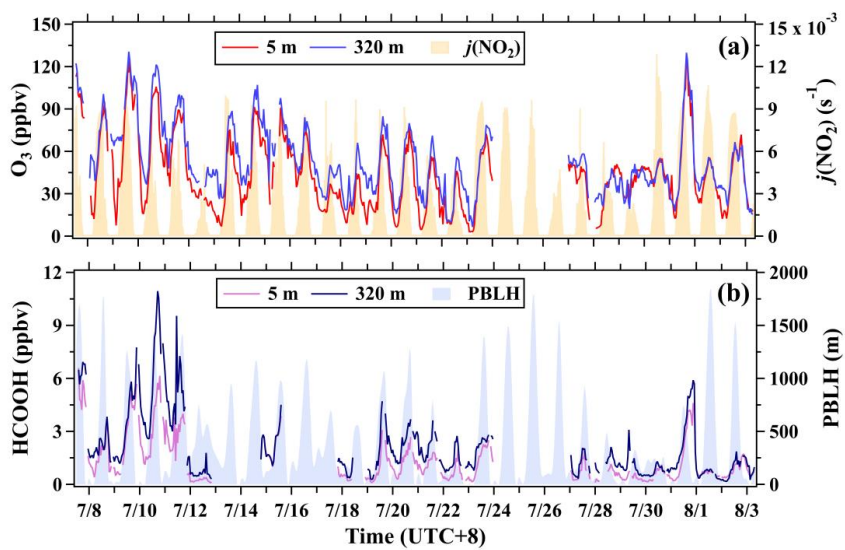
1000

1001 **Figure 2.** Assessment of long tubes in measuring formic and isocyanic acids in ambient
1002 air. (a-b) Scatterplots of mixing ratios of formic and isocyanic acids measured with the
1003 400 m long tube versus those measured without the long tube. (c-d) Scatterplots of
1004 $\Delta[HCOOH]$ versus $\delta[HCOOH]$ and scatterplots of $\Delta[HNCO]$ versus $\delta[HNCO]$ for
1005 the 100, 200, 300, and 400 m tubes.



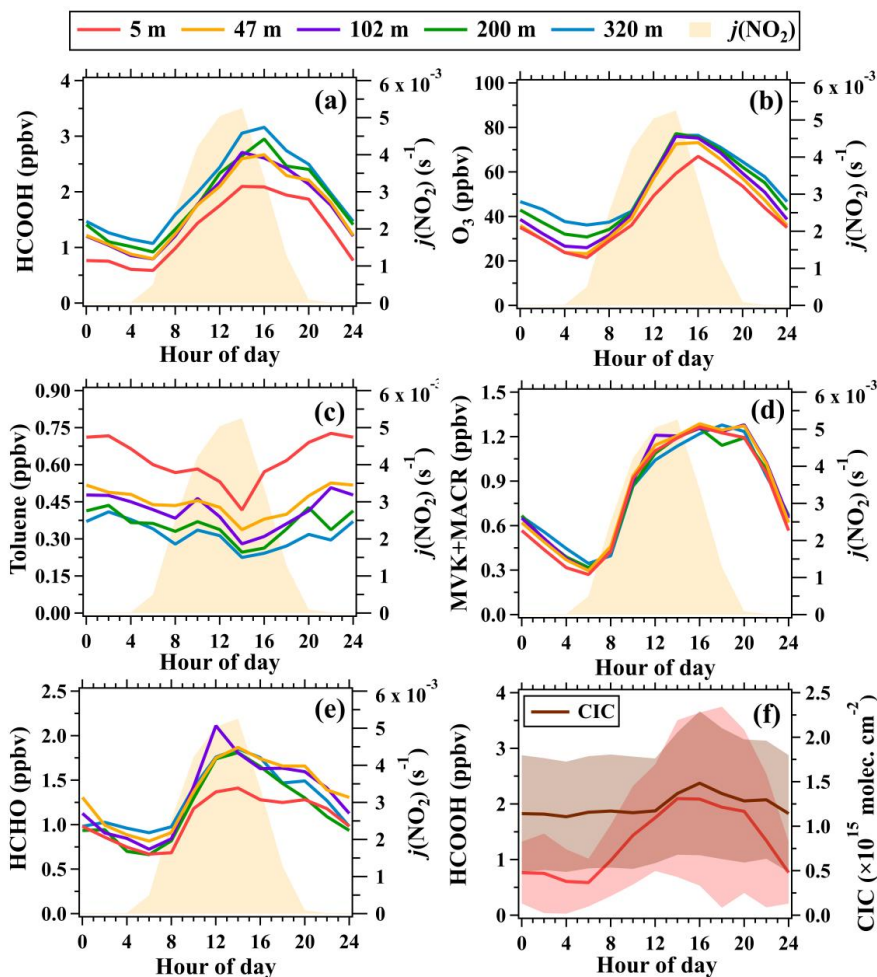
1006

1007 **Figure 3.** Linear fitting parameters (namely k and R^2) for (a) $\Delta[HCOOH]$ versus
1008 $\delta[HCOOH]$ and (b) $\Delta[HNCO]$ versus $\delta[HNCO]$. The scatterplots are shown in
1009 Figure 2. k and R^2 are the slope and determination coefficient of the linear fitting lines,
1010 respectively.



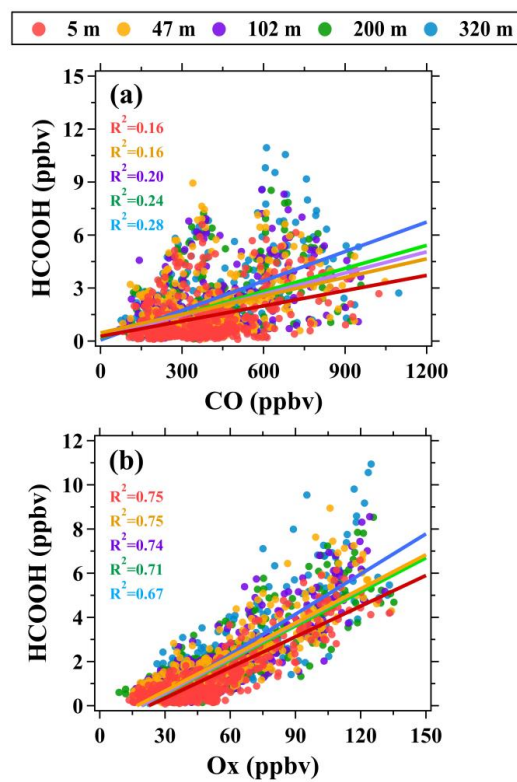
1011

1012 **Figure 4.** Time series of (a) O₃ (5 and 320 m), $j(\text{NO}_2)$, (b) formic acid (5 and 320 m),
1013 and planetary boundary layer height (PBLH) during the campaign.



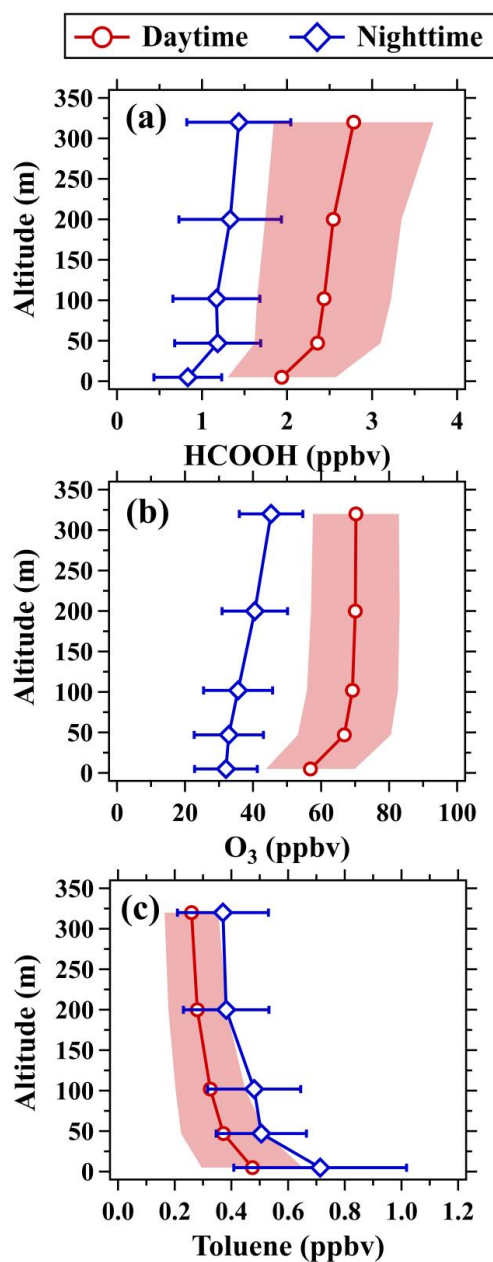
1014

1015 **Figure 5.** Average diurnal variations in mixing ratios of (a) formic acid, (b) O₃, (c)
1016 toluene, (d) MVK+MACR and (e) formaldehyde at 5, 47, 102, 200, and 320 m. (f)
1017 Average diurnal variations in mixing ratios (5 m) and CICs of formic acid during the
1018 field campaign; The shaded areas in panel (e) are half of the standard deviations.

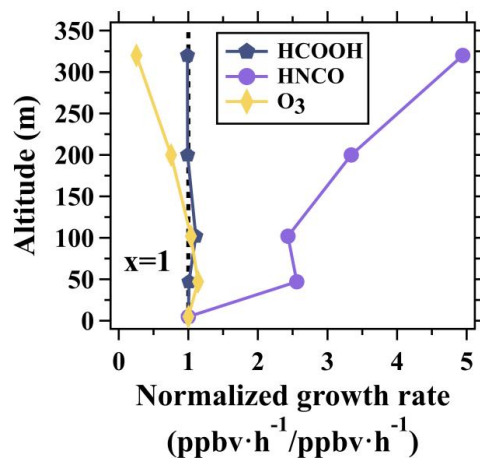


1019

1020 **Figure 6.** Scatter plots of (a) formic acid versus CO and (b) formic acid versus Ox at
1021 different altitudes during the campaign.



1022
1023 **Figure 7.** Vertical profiles of (a) formic acid, (b) O₃, and (c) toluene in daytime (11:00-
1024 16:00 LT) and nighttime (22:00-5:00 LT). The shaded areas and error bars are half of
1025 the standard deviations.

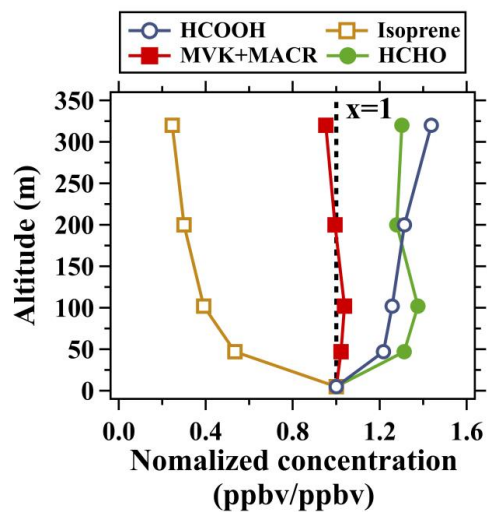


1026

1027 **Figure 8.** Normalized vertical profiles of the growth rates of ozone, formic acid, and

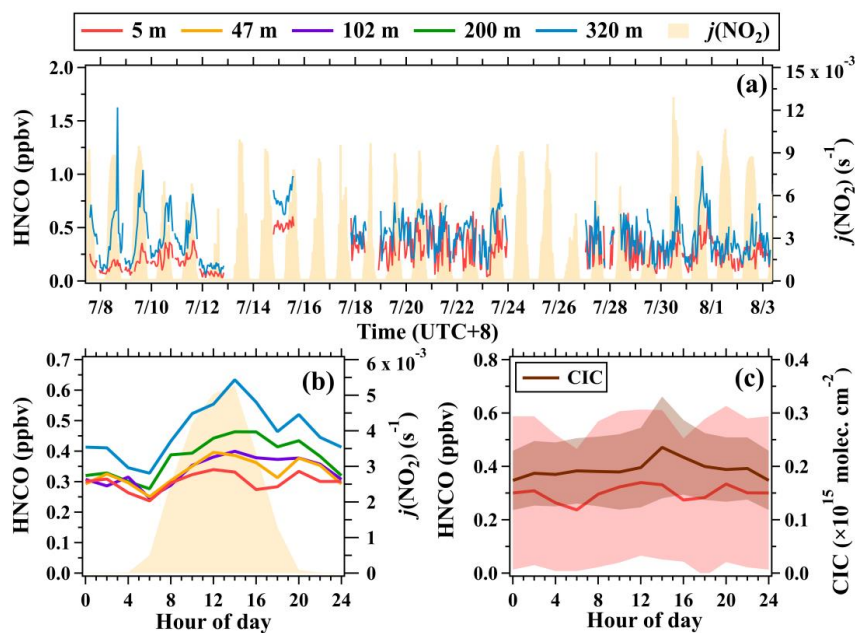
1028 isocyanic acid between 6:00-10:00 LT averaged over the whole campaign. Growth rates

1029 of the species at different altitudes were normalized to those at 5 m.



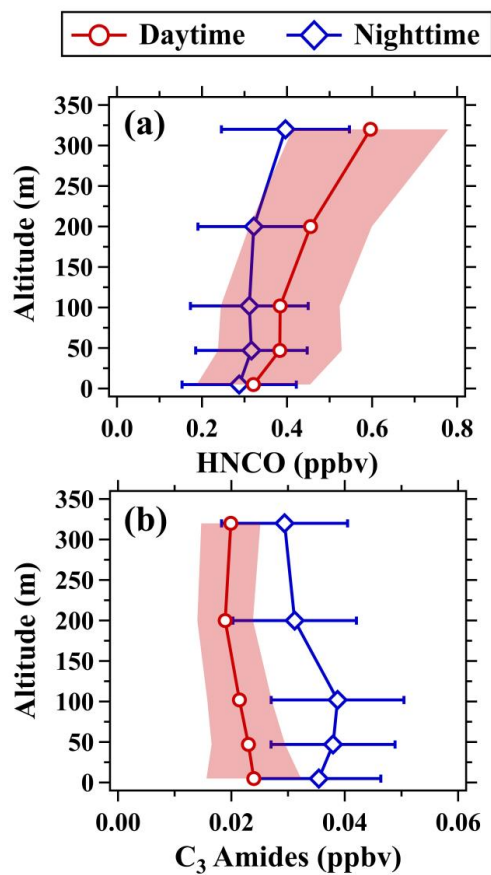
1030

1031 **Figure 9.** Normalized vertical profiles of formic acid, isoprene, formaldehyde, MVK
1032 and MACR in daytime (11:00-16:00 LT) averaged over the whole campaign. Mixing
1033 ratios of the species at different altitudes were normalized to those at 5 m.



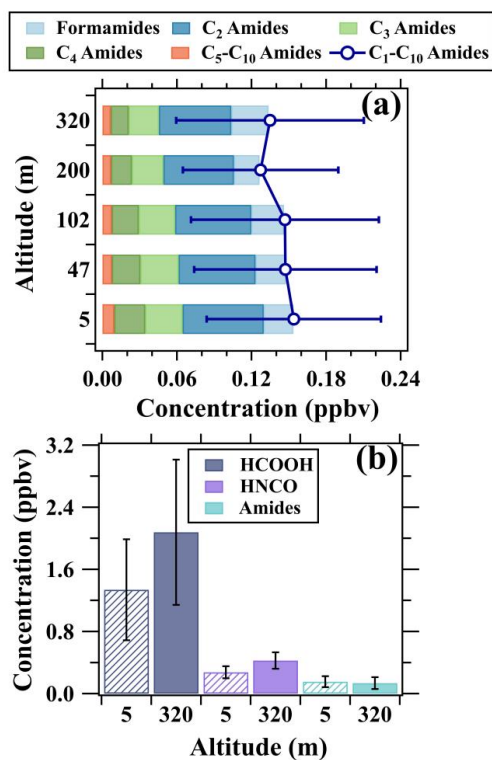
1034

1035 **Figure 10.** (a) Time series of isocyanic acid (5 and 320 m) and $j(\text{NO}_2)$. (b) Average
1036 diurnal variations in isocyanic acid at 5, 47, 102, 200, and 320 m. (c) Average diurnal
1037 variations in mixing ratios (5 m) and CICs of isocyanic acid during the campaign; The
1038 shaded areas in panel (c) are half of the standard deviations.



1039

1040 **Figure 11.** Vertical profiles of (a) isocyanic acid and (b) C₃ amides in daytime (11:00-
1041 16:00 LT) and nighttime (22:00-5:00 LT). The shaded areas and error bars are half of
1042 the standard deviations.



1043

1044 **Figure 12.** (a) Vertical variations in composition and concentrations of amides. (b)

1045 Concentration comparison of formic acid, isocyanic acid, and amides between 5 and

1046 320 m. The data in both (a) and (b) was the average results of the whole campaign.